# Mapping of the Spectral Densities of N–H Bond Motions in Eglin *c* Using Heteronuclear Relaxation Experiments†

Jeffrey W. Peng‡,§ and Gerhard Wagner*,‡

*Department of Biological Chemistry and Molecular Pharmacology, Harvard Medical School, 240 Longwood Avenue, Boston, Massachusetts 02115, and Biophysics Research Division, University of Michigan, 2200 Bonisteel Boulevard, Ann Arbor, Michigan 48109*

*Received April 17, 1992; Revised Manuscript Received June 10, 1992*

ABSTRACT: A new strategy is used for studying the internal motions of proteins based on measurements of NMR relaxation parameters. The strategy yields values of the so-called spectral density functions $J(\omega)$ for N–H bond vectors. The spectral density functions are related to the distribution of frequencies contained in the rotational (overall and internal) motions of these NH bond vectors. No a priori model assumptions about the dynamics are required in this approach. The method involves measurements of six relaxation parameters consisting of $^{15}N$ longitudinal relaxation rates, transverse relaxation rates of in-phase and antiphase coherence, the relaxation rates of heteronuclear $^{1}H$–$^{15}N$ two-spin order, the heteronuclear $^{1}H$–$^{15}N$ nuclear Overhauser effects, and longitudinal relaxation rates of the amide protons. The values of the spectral density functions at the five frequencies 0, $\omega_N$, $\omega_H + \omega_N$, $\omega_H$, and $\omega_H - \omega_N$ are determined from the relaxation parameters using analytical relations derived previously [Peng & Wagner (1992) *J. Magn. Reson. 98*, 308–332]. Here, the method is applied to characterize the backbone dynamics of the $^{15}N$-enriched proteinase inhibitor eglin *c*, a protein of 70 residues. The values for $J(0)$ and $J(\omega_N = 50$ MHz) vary significantly with the amino acid sequence, whereas the spectral densities at higher frequencies, $J(450$ MHz), $J(500$ MHz), and $J(550$ MHz), are typically much smaller and show no significant variation with the sequence. The collective behavior of the $J(\omega)$ values indicate greater internal motion for the proteinase binding loop residues and the first eight N-terminal residues. The additional internal motion in these regions is in the rate range below 450 MHz. The values of $J(\omega)$ are also compared with root mean square deviations (rmsds) of backbone atoms as obtained in NMR structure determinations. Low values of $J(0)$ and $J(\omega_N)$ are correlated with high rmsds. Spectral densities at higher frequencies, $J(450$ MHz), $J(500$ MHz), and $J(550$ MHz), are small and show no correlation with rmsds. A comparison with the spectral density functions obtained by fitting the experimental data to the functional dependence of the Lipari and Szabo formalism [Lipari & Szabo (1982a) *J. Am. Chem. Soc. 104*, 4546–4559] is made.

The study of protein dynamics in solution using two-dimensional (2D) NMR[1] methods has been the focus of increasing attention. This stems from at least two motivations. First, there is an intrinsic interest in determining whether correlations exist between protein function and dynamics. Theoretical studies suggest that local fluctuations of the protein architecture may be an integral component to the proper functioning of the protein molecule (Karplus & McCammon, 1981; McCammon & Harvey, 1987; Brooks et al., 1988). Second, molecular dynamics concepts and algorithms are being used more frequently to refine proposed NMR structures (Brünger et al., 1986; Nilges et al., 1988a,b; Clore & Gronenborn, 1989). In these structural studies, it would be useful to know how the apparent precision of a structure may be affected, if one acknowledges the existence of protein mobility.

The study of protein dynamics by 2D NMR has been accelerated by the increasing availability of isotopically labeled samples and the resolution afforded by 2D heteronuclear correlation spectroscopy. Together, these factors allow the spectroscopist to obtain a large number of heteronuclear ($^{15}N$, $^{13}C$) relaxation parameters for the protein. Since the heteronuclear relaxation rates depend chiefly on the dynamics of the heteronucleus–proton bond vectors with respect to the external magnetic field, the motions of these bond vectors can be characterized (Allerhand et al., 1971). Thus, the dynamics of the protein backbone can be monitored using a complete set of amide $^{15}N$ or $^{13}C^{\alpha}$ relaxation parameters.

The transcription of heteronuclear NMR relaxation data into dynamics information typically involves three steps. First, the dominant relaxation mechanisms and kinetics relevant to the spin systems under study are identified. For amide $^{15}N$–$^{1}H$ backbone studies, these mechanisms typically include the heteronuclear dipolar interaction between the $^{15}N$ and $^{1}H$ nuclei and the chemical shift anisotropy (CSA) interaction between the applied magnetic field $\mathbf{B}_0$ and the $^{15}N$ nuclear magnetic moments (Kay et al., 1989; Clore et al., 1990a,b). Second, the appropriate heteronuclear pulse sequences must be chosen to accurately measure the desired relaxation processes. Presently, relaxation studies of proteins typically involve the measurement of the longitudinal relaxation rate $1/T_1$, transverse relaxation rates $1/T_2$, and heteronuclear NOEs, which are related to heteronuclear cross-relaxation rates (Kay et al., 1989; Clore et al., 1990a,b; Palmer et al., 1991a,b). Finally, a method must be employed to relate the observed relaxation rates to the motional properties of the system.

The last step proves difficult with the current methods employed. In particular, the information obtained from the $1/T_1$, $1/T_2$, and heteronuclear NOE measurements is not

† This work was supported by NSF Grant DMB-9007878 and NIH Grant T32-GM08270-32 for part of the salary to J.P.

* Author to whom correspondence should be addressed.
‡ Harvard Medical School.
§ University of Michigan.

[1] Abbreviations: CSA, chemical shift anisotropy; GARP, globally optimized alternating phase rectangular pulse; INEPT, insensitive nuclei enhancement by polarization transfer; MHz, megahertz; NMR, nuclear magnetic resonance; NOE, nuclear Overhauser effect; rmsd, root mean square deviation; TPPI, time proportional phase incrementation.

0006-2960/92/0431-8571$03.00/0 

sufficient to characterize the bond dynamics without first making some a priori model assumptions about the dynamics itself. To overcome this difficulty, an assortment of motional models for the dynamics of XH bonds in proteins or models with preassumed analytical dependencies on certain parameters have been presented in the literature (Woessner, 1962; Kinoshita et al., 1977; Richarz et al., 1980; King & Jardetzky, 1978; King et al., 1978; Ribeiro et al., 1980; Jardetzky & Roberts, 1981; Lipari & Szabo, 1982a,b; Clore et al., 1990a,b). All of these models are based on the assumption that the autocorrelation function for the XH bond motion can be described as a sum of exponential decays, or, equivalently, the spectral density function is a sum of Lorentzian curves (vide infra). Each of these models supplies a set of motional parameters which one adjusts in a least-squares fitting procedure to reproduce the observed relaxation data. One then uses the optimized motional parameters to make conclusions about the protein dynamics. While these models may, in fact, be quite reasonable, it is clearly desirable to remove the necessity of introducing model assumptions to interpret the relaxation data in a motional context.

Here, we use an alternative approach that directly exploits the dynamic information contained in the relaxation rates (Peng & Wagner, 1992). It is well-known that dynamics information in the heteronuclear relaxation parameters enters through their dependence on the spectral density functions, $J(\omega)$, for the associated heteronucleus–proton bond motions. Specifically, the relaxation rates depend on a weighted sum of the $J(\omega)$ sampled at specific frequencies. For example, in an amide $^{15}N$–$^{1}H$ spin system, these include samplings at 0, $\omega_N$, $\omega_{H^N}$, and $\omega_{H^N} \pm \omega_N$, where $\omega_N$ and $\omega_{H^N}$ are the angular Larmor frequencies for the $^{15}N$ and amide $^{1}H$ spins, respectively. The form of the $J(\omega)$ is dictated by the dynamics of these bonds; therefore, the central aim of the heteronuclear relaxation studies is to characterize the shapes of the individual spectral density functions. As described above, the use of a motional model amounts to proposing an analytical form for the $J(\omega)$. This is necessary in approaches using only $1/T_1$, $1/T_2$, and the NOE measurements, since the information content of three relaxation parameters is not sufficient to determine the spectral densities at any of the five sampling frequencies. However, by measuring an expanded set of relaxation parameters which include not only $1/T_1$, $1/T_2$, and the NOE but two-spin relaxation rates as well, these samplings of $J(\omega)$ can be obtained from experiment. No model assumptions about the nature of the XH bond motions are necessary. We will refer to this approach of using the relaxation data to directly evaluate the spectral density functions at specific frequencies as "spectral density mapping".

Here, we have used spectral density mapping to characterize the backbone dynamics of the protein eglin *c*. Eglin *c* is a 70-residue inhibitor (MW = 8000) that binds to such proteinases as elastase, subtilisin, thermistase, and chymotrypsin. The crystal structure of eglin *c* in complex with subtilisin Carlsberg has been determined (McPhalen et al., 1985; Bode et al., 1986, 1987); no crystal structure of the free inhibitor is available yet. The solution structure of free eglin *c* has been determined by two-dimensional NMR methods (Hyberts & Wagner, 1990; Hyberts et al., 1992). The structural studies have revealed that some parts of the protein backbone are less well-ordered. This has been one of the motivations for studying the dynamic properties eglin *c*. Furthermore, the results presented here suggest that the dynamic properties of eglin *c* may have considerable relevance toward its function as a proteinase inhibitor.

## MATERIALS AND METHODS

*Protein Sample Preparation.* Samples of eglin *c* were produced from a synthetic gene that was cloned and expressed at high yield in *Escherichia coli* (Ciba-Geigy, Basel, Switzerland). $^{15}N$ labeling was achieved by growing up cells in media containing $^{15}N$-labeled ammonium chloride as the sole nitrogen source. The expressed eglin *c* is actually $N^{\alpha}$-acetyleglin *c* due to modification in a posttranslational event (Märki et al., 1985). Uniformly $^{15}N$-enriched eglin *c* (13.7 mg) was dissolved in 450 $\mu$L of a mixture of 95% $H_2O$ and 5% $D_2O$ for a concentration of 3.8 mM. The sample was degassed and the pH set to $\approx$3.0 for all relaxation measurements.

*NMR Spectroscopy.* All 2D spectra were recorded on a Bruker AMX 500 spectrometer at 36 °C. In accordance with methods detailed elsewhere (Peng & Wagner, 1992) a total of six relaxation parameters were measured for the backbone NH bonds of eglin *c*. We use the symbols $R_{obs}(Q)$ to refer to the specific relaxation rates. The "obs" refers to the type of nucleus or nuclei whose relaxation rates are being probed (either H, N, or both), and the $Q$ refers to the particular type of spin order undergoing relaxation in the experiment. We use the term spin order after the convention of Ernst et al. (1987) to describe generalized macroscopic spin states. Using this nomenclature, the measured rates included the longitudinal $^{15}N$ relaxation rate $R_N(N_z)$, the in-phase $^{15}N$ transverse relaxation rate $R_N(N_{x,y})$, the heteronuclear cross-relaxation rate $R_N(H_z^N \rightarrow N_z)$ via the heteronuclear NOE, the antiphase transverse relaxation rate $R_{NH}(2H_z^N N_{x,y})$, the decay rate of longitudinal two-spin order $R_{NH}(2H_z^N N_z)$, and the amide proton longitudinal relaxation rate $R_H(H_z^N)$. The 2D pulse sequences used to measure these rates have been described previously (Peng & Wagner, 1992). The only modifications in this study included the omission of the proton 180° pulse in the center of the relaxation delay for the $R_{NH}(2H_z^N N_z)$ experiment and an improved compensation for the phase offsets between the low- and high-power output of the X-nucleus ($^{15}N$) amplifier in the transverse relaxation experiments. The sequences are all based on double INEPT or refocused INEPT heteronuclear correlation sequences with relaxation delays appropriately inserted. The GARP broadband decoupling scheme (Shaka et al., 1985) was applied to the $^{15}N$ spins during detection in all experiments. Further discussions of these or similar pulse sequences are given in the literature (Nirmala & Wagner, 1988, 1989; Kay et al., 1989; Palmer et al., 1991). In all of the sequences, a particular state of nonequilibrium spin order is created for the NH spin systems and allowed to relax for a variable period $T$. The residual spin order is then identified with the intensity of a cross-peak at frequency coordinates defined by the chemical shifts of the $^{15}N$ and the attached proton. The 2D data sets consisted of 2048 real data points for 128 $t_1$ blocks. The $^{15}N$ sweep width was set to 2000 Hz. Sixteen scans were acquired per free induction decay, except for the NOE measurements which used more scans owing to the lack of an initial polarization transfer. In all cases, sign discrimination in the $^{15}N$ dimension ($F_1$) was achieved by the TPPI method of Marion and Wüthrich (1983). Measuring time for the longitudinal $^{15}N$ relaxation rate $R_N(N_z)$ and NOE experiments were typically 2–4 days. The other relaxation series took typically a day to record nine spectra for nine distinct relaxation delays. The total relaxation delay between scans was 3 s, which included 1.3 s of solvent presaturation.

The $R_N(N_z)$ values were obtained with 11 delays of 10, 50, 100, 150, 200, 300, 400, 500, 800, 2000, and 3000 ms. $R_N(N_{x,y})$ values were obtained with 10 delays of 6.4, 6.4, 12.8,

25.6, 38.4, 51.2, 76.8, 102.4, 140.8, and 179.2 ms. The $R_{NH}(2H_z^N N_{x,y})$ measurements used 8 delays of 6.4, 12.8, 25.6, 51.0, 76, 102.4, 134, and 172.8 ms. In these experiments, the continuous-wave $^{15}N$ spin lock power was set to 2500 Hz, resulting in an effective field tipped at 77° from the laboratory $z$ axis for resonances at the extreme edges of the spectrum. The $R_{NH}(2H_z^N N_z)$ measurements were obtained from 9 delays of 2, 10, 20, 30, 50, 70, 100, 130, and 170 ms. Amide proton spin–lattice relaxation rates $R_H(H_z^N)$ used 10 delays of 0.001, 10, 10, 20, 30, 40, 50, 70, 100, and 125 ms. Finally, the heteronuclear NOEs were obtained by recording three spectra with 3 s of proton saturation and two spectra without proton saturation. The difference in cross-peak intensities between the two sets of spectra then yielded the NOE values. All 2D datasets were processed on both SUN SLC and IRIS 4D-35 workstations using FELIX 1.0 software provided by Dennis Hare (Hare Research, Seattle); 60° shifted sine squared window functions were used prior to Fourier transformation. Free induction decays along $t_2$ were strip transformed and zero-filled to 1024 real points. Interferograms along $t_1$ were zero-filled twice to a length of 512 real points. An example of a representative 2D spectrum is given in an earlier related study on eglin $c$ (Peng et al., 1991a). Assignments of the cross-peaks have been obtained using standard methods and will be published elsewhere (Peng and Wagner, unpublished results).

*Determination of Relaxation Rates.* Cross-peaks of the 2D spectra were integrated along slices through the $^1H$ ($F_2$) dimension corresponding to the cross-peak maxima. The slices were subject to a linear baseline correction prior to integration. For each amide $^{15}N$–$^1H$ cross-peak, a data file of peak integral vs relaxation delay, $T$, was obtained. The data files were then fit to exponential decays using the Levenburg–Marquardt algorithm (Marquardt, 1963; Press et al., 1988). For the $R_N(N_z)$ the time dependence of the peak intensity $I$ is taken to follow the three-parameter expression

$$I(T) = A + B \exp[-R_N(N_z)T] \quad (1)$$

The initial value for the peak intensity is $(A + B)$, and the steady-state value is $A$. For the remaining experiments, the time dependence is assumed to be well-described by the simpler two-parameter exponential decay

$$I(T) = A \exp[-R_{obs}(Q)T] \quad (2)$$

Uncertainties in the fitted rates due to random errors were estimated using established Monte Carlo procedures (Kamath & Shriver, 1989; Palmer et al., 1991a,b; Kay et al., 1992). The values of the cross-peak integrals were assumed to be the means of Gaussian distributions. The root mean square deviations between the experimental data and the optimized fits were used for the standard deviations of the Gaussians. An ensemble of 500 synthetic data sets were generated for each residue. For each of the 500 synthetic data sets relaxation rates were obtained using the same Levenburg–Marquardt fitting procedures. The estimated errors in the relaxation rates were taken to be the standard deviations derived from the ensemble of simulated data.

The applicability of using Gaussian standard deviations based on those from the optimized fits was checked by estimating the uncertainties in the one-dimensional cross-peak integrals. A series of ≈100 integrals were measured along rows devoid of peaks in each spectra of each series. The standard deviation of these integrals was taken as an approximation for the uncertainty in the integral values. Typically, spectra correspondng to the shorter relaxation delays gave larger uncertainty estimates. However, in all of the relaxation experiments, the uncertainties in the integrals derived from these spectra were typically of the same magnitude or less than those derived from the fitting routine. Thus, the use of standard deviations derived from the fitting routines does not appear to underestimate the effects of random errors.

## RESULTS

*Theoretical Background.* Before the results are discussed, it is useful to outline the connection between the spectral density values, the $^{15}N$ NMR relaxation parameters, and molecular motion. The heteronuclear relaxation rates give information about the rotational fluctuations of the amide $^{15}N$–$^1H$ bond vectors with respect to the external magnetic field, $\mathbf{B}_0$. These fluctuations are due to both the overall tumbling of the protein molecule and any internal mobility as well. The fluctuations of each NH vector are described in terms of an angular autocorrelation function, $G(\tau)$ (Abragam, 1961). $G(\tau)$ describes the decay of correlations in an ensemble of molecules between the orientations of the NH vectors (in the laboratory frame) at two arbitrary instances separated by a delay $\tau$. For proteins in solution, it can be shown (Wittebort & Szabo, 1978; Lipari & Szabo, 1982a) that $G(\tau)$ is given simply by

$$G(\tau) = {}^1/_5\langle 1/2(3(\cos\theta(\tau))^2 - 1)\rangle \quad (3)$$

In the above expression, $\cos\theta(\tau)$ is the projection of a unit vector pointing along the NH vector at a time $t$ and onto itself at a time $t + \tau$ later. The angled brackets denote an ensemble average, and therefore the enclosed trigonometric function is averaged for the particular NH vector over all protein molecules in solution. For $\tau = 0$, the NH vector has not moved so $\cos\theta = 1$ and $G(0) = 1/5$. As $\tau$ increases, the NH vector undergoes motion such that, on average, $\cos\theta$ is less than 1, and therefore the ensemble average of eq 3 decreases, resulting in a decrease of $G(\tau)$. Note that this motion will include the effects of both overall tumbling and internal motion. In the limit of $\tau = \infty$, $G(\tau) = 0$ since the ensemble average over all molecules reduces to an average of the overall possible angles $\theta$. In practical terms, $G(\tau)$ decays to 0 after some characteristic length of time, and all delays $\tau$ greater than this length are considered infinite. The characteristic length of $G$ can be defined by computing the area under $G(\tau)$ (from 0 to ∞) and dividing by the initial value $G(0)$ (Friedman, 1985; Chandler, 1987). This characteristic length is often called the "correlation time" or "coherence time" $\tau_c$ of the motion. The correlation time $\tau_c$ sets the time scale on which random fluctuations in the NH vector orientation occur. In this general form, a correlation time is defined independently from a motional model.

All amide NH vectors have the boundary values of $G(0) = 1/5$ and $G(\infty) = 0$; these values are independent of the specific dynamics. Instead, the manner in which $G(\tau)$ decays depends on the dynamics of the specific NH vector. Therefore, we are interested in describing the temporal decay of $G(\tau)$. This description is achieved by a spectral analysis of the rotational fluctuations. In particular, one takes the Fourier cosine transform of $G(\tau)$ (Abragam, 1961; Wittebort & Szabo, 1978).

$$J(\omega) = 2\int_0^\infty \cos(\omega\tau)G(\tau)\,d\tau \quad (4a)$$

The result, $J(\omega)$, is called the spectral density of the NH fluctuations. The cosine transform filters $G(\tau)$ for changes occurring on the range of time scales defined by $\tau = 2\pi/\omega$.

The result gives the relative contribution that frequencies in the range $(\omega, \omega + d\omega)$ make toward $G(\tau)$.

Each NH vector has a spectral density function $J(\omega)$ that gives the distribution of frequencies contained in the rotational fluctuations of the same NH vector. NH vectors with different mobilities will have different shapes for $J(\omega)$. For example, NH vectors which reorient faster will have autocorrelations $G(\tau)$ that decay more rapidly, resulting in a broader distribution for $J(\omega)$. This is apparent from the Fourier transform relationship in eq 4. A broader shape for $J(\omega)$ implies an increase of higher frequency motions for the NH vector. Although the width of $J(\omega)$ increases for more mobile NH vectors, the area under $J(\omega)$ remains invariant (Slichter, 1978). The invariance reflects the fact that the energy of the local magnetic fields causing relaxation (i.e., dipolar or CSA) has a constant value over the ensemble (Abragam, 1961). Thus, $J(\omega)$ expresses how this value is distributed over a spectrum of frequencies, and this depends on the individual dynamics of the NH vectors. $J(0)$ has a special meaning. It represents the area under the correlation function $G(\tau)$ and is therefore proportional to the generalized correlation time $\tau_c$ defined as

$$J(0) = 2\int_0^\infty G(\tau)\, d\tau = 2\, G(0)\tau_c = {}^2/_5\tau_c \qquad (4b)$$

Essentially, the inverse of $J(0)$ measures the width of the distribution of frequencies contained in the fluctuations. Smaller $J(0)$ values are correlated with broader $J(\omega)$ distributions, and larger $J(0)$ are correlated with narrower distributions. Equivalently, smaller $J(0)$ values imply shorter $\tau_c$ values and, therefore, more rapid rotational fluctuations of the NH vector. Note that $J(0)$ is simply the limiting value of the spectral density function for time scales in which the autocorrelation have already decayed to 0. Thus, the maximum value of $J(0)$ will be determined by the overall rotational diffusion of the protein. It is important to note that the above properties of $J(\omega)$ give us information about the NH dynamics, without the need for a priori model assumptions about the dynamics. In particular, the $J(\omega)$ values reflect both the global and internal motions of the protein; no assumptions are made about the separability of time scales between such motions.

The orientational fluctuations of the NH vectors, due to both overall tumbling and internal motion, generate the local time-varying magnetic fields at the $^{15}N$ and $^1H$ nuclei. These fields constitute the relaxation mechanisms of the NH spin systems. As with previous studies of $^{15}N$ relaxation, we consider the local fields from the heteronuclear dipolar interaction between the $^{15}N$ and the amide $^1H$, as well as the CSA interaction between the $^{15}N$ and the applied field $\mathbf{B}_0$ (Kay et al., 1989; Clore et al., 1990a,b). Since these fields are driven by molecular motion, the frequency content available in these fields is simply the spectral densities $J(\omega)$ of the NH fluctuations. The rate of relaxation depends critically on the extent of overlap between the band of frequencies contained in $J(\omega)$ and the sharp transition frequencies selected by the NH spin system which include 0, $\omega_N$, $\omega_{H^N}$, and $\omega_{H^N} \pm \omega_N$ (Abragam, 1961; Ernst et al., 1987; Goldman, 1988). In effect, the values of the relaxation rates probe the spectral densities at these specific frequencies, and hence, dynamics information about the NH vectors is communicated to the relaxation rates.

In accordance with the above discussion, the relaxation rates germane to the NH spin systems are linear combinations of the spectral densities sampled at 0, $\omega_N$, $\omega_{H^N}$, $\omega_{H^N} + \omega_N$ and $\omega_{H^N} - \omega_N$. In our 500-MHz spectrometer these frequencies correspond to 0, 50.68, 449.46, 500.14, and 550.82 MHz, respectively. Since the gyromagnetic ratio of $^{15}N$ is negative, $\omega_{H^N} + \omega_N$ is at 449.46 MHz and $\omega_{H^N} - \omega_N$ is at 550.82 MHz.

The manner in which the relaxation rates sample the spectral density function has been illustrated schematically in earlier studies (Wagner & Nirmala, 1989; Peng et al., 1991a; Peng & Wagner, 1992). Hereafter, we will commonly refer to $J(0)$ and $J(\omega_N)$ as the lower frequency spectral density values and $J(\omega_{H^N} - \omega_N)$, $J(\omega_{H^N})$, and $J(\omega_{H^N} + \omega_N)$ as the higher frequency spectral density values. The specific linear combination of spectral densities depends on the type of spin order undergoing relaxation. For the single spin $^{15}N$ relaxation rates one finds for $1/T_1$, $1/T_2$, and the heteronuclear cross-relaxation rate the well-known relations (Abragam, 1961)

$$R_N(N_z) = \frac{\gamma_{H^N}^2\gamma_N^2\hbar^2}{4r_{NH^N}^6}\{J(\omega_{H^N}-\omega_N) + 3J(\omega_N) + 6J(\omega_{H^N}+\omega_N)\} + \frac{\Delta^2\omega_N^2}{3}J(\omega_N) \qquad (5)$$

$$R_N(N_{x,y}) = \frac{\gamma_{H^N}^2\gamma_N^2\hbar^2}{8r_{NH^N}^6}\{4J(0) + J(\omega_{H^N}-\omega_N) + 3J(\omega_N) + 6J(\omega_{H^N}) + 6J(\omega_{H^N}+\omega_N)\} + \frac{\Delta^2\omega_N^2}{3}\left\{\frac{2}{3}J(0) + \frac{1}{2}J(\omega_N)\right\} \qquad (6)$$

$$R_N(H_z^N\rightarrow N_z) = \frac{\gamma_{H^N}^2\gamma_N^2\hbar^2}{4r_{NH^N}^6}\{6J(\omega_{H^N}+\omega_N) - J(\omega_{H^N}-\omega_N)\} \qquad (7)$$

The cross-relaxation rate and the longitudinal relaxation rate combine to give the steady-state heteronuclear NOE ($\eta$) defined by

$$\eta = \frac{I_{sat} - I_{eq}}{I_{eq}} = \frac{\gamma_H}{\gamma_N}\frac{R_N(H_z^N\rightarrow N_z)}{R_N(N_z)} \qquad (8)$$

This definition of $\eta$ as the steady-state NOE is that of Noggle and Schirmer (1971). $I_{sat}$ is the cross-peak intensity with proton saturation, and $I_{eq}$ is the equilibrium Zeeman intensity. NOE values consistent with definitions given in previous studies of $^{15}N$ protein relaxation are obtained by using $(1 + \eta)$ (Kay et al., 1989; Clore et al., 1990a,b). The two-spin relaxation rates (Goldman, 1988; Bax et al., 1990; Boyd et al., 1990; Peng et al., 1991a,b; Peng & Wagner, 1992) are given by

$$R_{NH}(2H_z^NN_z) = \frac{\gamma_{H^N}^2\gamma_N^2\hbar^2}{4r_{NH^N}^6}\{3J(\omega_N) + 3J(\omega_{H^N})\} + \frac{\Delta^2\omega_N^2}{3}J(\omega_N) + \rho_{H^NH^i} \qquad (9)$$

$$R_{NH}(2H_z^NN_{x,y}) = \frac{\gamma_{H^N}^2\gamma_N^2\hbar^2}{8r_{NH^N}^6}\{4J(0) + J(\omega_{H^N}-\omega_N) + 3J(\omega_N) + 6J(\omega_{H^N}+\omega_N)\} + \frac{\Delta^2\omega_N^2}{3}\left\{\frac{2}{3}J(0) + \frac{1}{2}J(\omega_N)\right\} + \rho_{H^NH^i} \qquad (10)$$

where $\rho_{H^NH^i}$ is the sum of rates

$$\rho_{H^NH^i} = \sum_i \frac{\gamma_{H^N}^2\gamma_{H^i}^2\hbar^2}{4r_{H^NH^i}^6}\{J_{H^NH^i}(\omega_{H^N}-\omega_{H^i}) + 3J_{H^NH^i}(\omega_{H^N}) + 6J_{H^NH^i}(\omega_{H^N}+\omega_{H^i})\} \qquad (11)$$

In the above expressions, $\gamma_N$ and $\gamma_{H^N}$ are the gyromagnetic ratios for the $^{15}N$ and amide proton nuclei. $\hbar$ is Planck's

constant divided by $2\pi$, and $r_{NH^N}$ is the length of the NH bond vector. The $r_{H^NH^i}$ values are the lengths of interspin vectors connecting a given amide $H^N$ proton with other distinct protons $H^i$. $\omega_N$ is the Larmor frequency of the $^{15}N$ nucleus in radians per second, and $\Delta$ is the chemical shift anisotropy value for an axially symmetric shift tensor (Wittebort & Szabo, 1978). The $^{15}N$ shift tensor is reported to be approximately symmetric with a symmetry axis nearly coincident with the NH bond vector (Hiyama et al., 1988). The relaxation rates for the two-spin orders $R_{NH}(2H_z^NN_z)$ and $R_{NH}(2H_z^NN_{x,y})$ are complicated by a significant dependence on the spin–lattice relaxation rate of the attached amide proton via the $\rho_{H^NH^i}$ term. To this end, a sixth relaxation measurement for the amide proton, $H^N$, longitudinal magnetization is required. The corresponding rate is given by

$$R_H(H_z^N) = \frac{\gamma_{H^N}^2\gamma_N^2\hbar^2}{4r_{NH^N}^6}\{J(\omega_{H^N}-\omega_N) + 3J(\omega_{H^N}) + 6J(\omega_{H^N}+\omega_N)\} + \rho_{H^NH^i} \quad (12)$$

The system of linear equations (eqs 5–10, 12) can be solved to obtain the spectral density values immediately from the experimental rates. These formulas are given as (Peng & Wagner, 1992)

$$J(0) = \frac{3}{4}\frac{1}{3d+c}\left\{-\frac{1}{2}R_N(N_z) + R_N(N_{x,y}) + R_{NH}(2H_z^NN_{x,y}) - \frac{1}{2}R_{NH}(2H_z^NN_z) - \frac{1}{2}R_H(H_z^N)\right\} \quad (13)$$

$$J(\omega_{H^N}-\omega_N) = \frac{1}{4}\frac{1}{d}\{R_N(N_z) - R_{NH}(2H_z^NN_z) + R_H(H_z^N) - 2R_N(H_z^N\rightarrow N_z)\} \quad (14)$$

$$J(\omega_N) = \frac{1}{2}\frac{1}{3d+c}\{R_N(N_z) + R_{NH}(2H_z^NN_z) - R_H(H_z^N)\} \quad (15)$$

$$J(\omega_{H^N}) = \frac{1}{12}\frac{1}{d}\{-R_N(N_z) + 2R_N(N_{x,y}) - 2R_{NH}(2H_z^NN_{x,y}) + R_{NH}(2H_z^NN_z) + R_H(H_z^N)\} \quad (16)$$

$$J(\omega_{H^N}+\omega_N) = \frac{1}{24}\frac{1}{d}\{R_N(N_z) - R_{NH}(2H_z^NN_z) + R_H(H_z^N) + 2R_N(H_z^N\rightarrow N_z)\} \quad (17)$$

The contribution of exclusively proton dipolar interactions to the amide proton spin–lattice relaxation rate is given by

$$\rho_{H^NH^i} = \left\{-\frac{1}{4}R_N(N_z) - \frac{1}{2}R_N(N_{x,y}) + \frac{1}{2}R_{NH}(2H_z^NN_{x,y}) + \frac{1}{4}R_{NH}(2H_z^NN_z) + \frac{1}{4}R_H(H_z^N)\right\} \quad (18)$$

The constants are defined as $d = \gamma_{H^N}^2\gamma_N^2\hbar^2/4r_{NH^N}^6$ and $c = \Delta^2\omega_N^2/3$. For a CSA value of $\Delta = -160$ ppm (Hiyama et al., 1988) and an internuclear $^{15}N$–$^1H$ bond distance of $r_{NH^N} = 1.02$ Å (Keiter, 1986), $d$ and $c$ become $\approx 1.3 \times 10^9$ (rad/s)$^2$ and $0.9 \times 10^9$ (rad/s)$^2$, respectively.

*Calculation of Model-Free Parameters.* The use of motional models to analyze the heteronuclear relaxation data means modeling the spectral density function. A particularly attractive formalism is the "model-free" approach of Lipari and Szabo (1982a,b). Their approach makes a minimum of assumptions about the NH vector dynamics and introduces a generalized order parameter that retains its physical interpretation for a variety of more specific models of motion. Their model of $J(\omega)$ is based on a very simple form for the autocorrelation function given by

$$G(\tau) = {}^1/_5G_o(\tau)G_i(\tau) \quad (19)$$

where

$$G_o(\tau) = \exp(-\tau/\tau_m) \quad (20)$$

and

$$G_i(\tau) = S^2 + (1 - S^2)\exp(-\tau/\tau_e) \quad (21)$$

After Fourier transformation as indicated in eq 4, the resulting spectral density is

$$J(\omega)_{ls} = \frac{2}{5}\left[\frac{S^2\tau_m}{1 + (\omega\tau_m)^2} + \frac{(1 - S^2)\tau_i}{1 + (\omega\tau_i)^2}\right] \quad (22)$$

Here, we have introduced the "ls" subscript to distinguish the Lipari and Szabo form for $J(\omega)$ from the spectral density values obtained from the relaxation rates. Equations 19–22 assume isotropic tumbling of the protein and that internal fluctuations of the NH vectors are independent of those due to molecular tumbling. $G_o(\tau)$ is the familiar monoexponentially decaying autocorrelation function for overall molecular tumbling (Abragam, 1961). $\tau_m$ is the overall rotational correlation time for molecular tumbling and therefore pertains to all residues. $G_i(\tau)$ is the autocorrelation function for the internal motions of a given NH vector with respect to a molecular-fixed frame. The parameters $S^2$ and $\tau_e$ contained in $G_i(\tau)$ are adjusted along with $\tau_m$ to best fit the observed relaxation data.

$S^2$ is the generalized order parameter and is the limiting value of $G_i(\tau)$ as $\tau$ goes to $\infty$. $S^2$ is interpreted as describing the amount of spatial freedom the NH vector has as a result of internal motion. If there are no restrictions on the internal motion, then $S^2$ is 0, and if there is no internal motion, $S^2$ is 1.0. In the limit that $S^2$ is unity, $J(\omega)_{ls}$ reduces to the familiar Lorentzian distribution for the rotational diffusion of a rigid, spherical tumbler (Abragam, 1961). $\tau_i$ is related to both $\tau_m$ and a so-called effective internal correlation time, $\tau_e$, through the relation

$$\frac{1}{\tau_i} = \frac{1}{\tau_m} + \frac{1}{\tau_e} \quad (23)$$

The $\tau_e$ values cannot be directly equated to microscopic time constants for the internal motion, since they generally depend on both the rate and amplitude of the internal motion (Lipari & Szabo, 1982a,b). Therefore, a physical interpretation of the $\tau_e$ values requires a more specific model of motion, such as the "wobbling in a cone" approach (Woessner, 1962; Kinoshita et al., 1977; Richarz et al., 1980). In this model, the NH vector is assumed to diffuse in a cone of semiangle $\alpha$, which is related to $(S^2)^{1/2}$ through the relation (Lipari & Szabo, 1982a,b)

$$S = {}^1/_2(\cos\alpha)(1 + \cos\alpha) \quad (24)$$

The microscopic time constant for diffusion in this cone can be extracted from the product $(1 - S^2)\tau_e$ (Lipari & Szabo, 1982a,b).

*Summary of Relaxation Rates for Eglin c.* The values of the relaxation parameters for eglin c are displayed in the bar graphs of Figure 1. Listings of the relaxation rates and estimated errors are provided in the supplementary material. Eglin c has 6 proline residues, and therefore, the relaxation rates of 64 NH vectors can be measured in principle. However, significant cross-peak overlap exists for two pairs of residues,

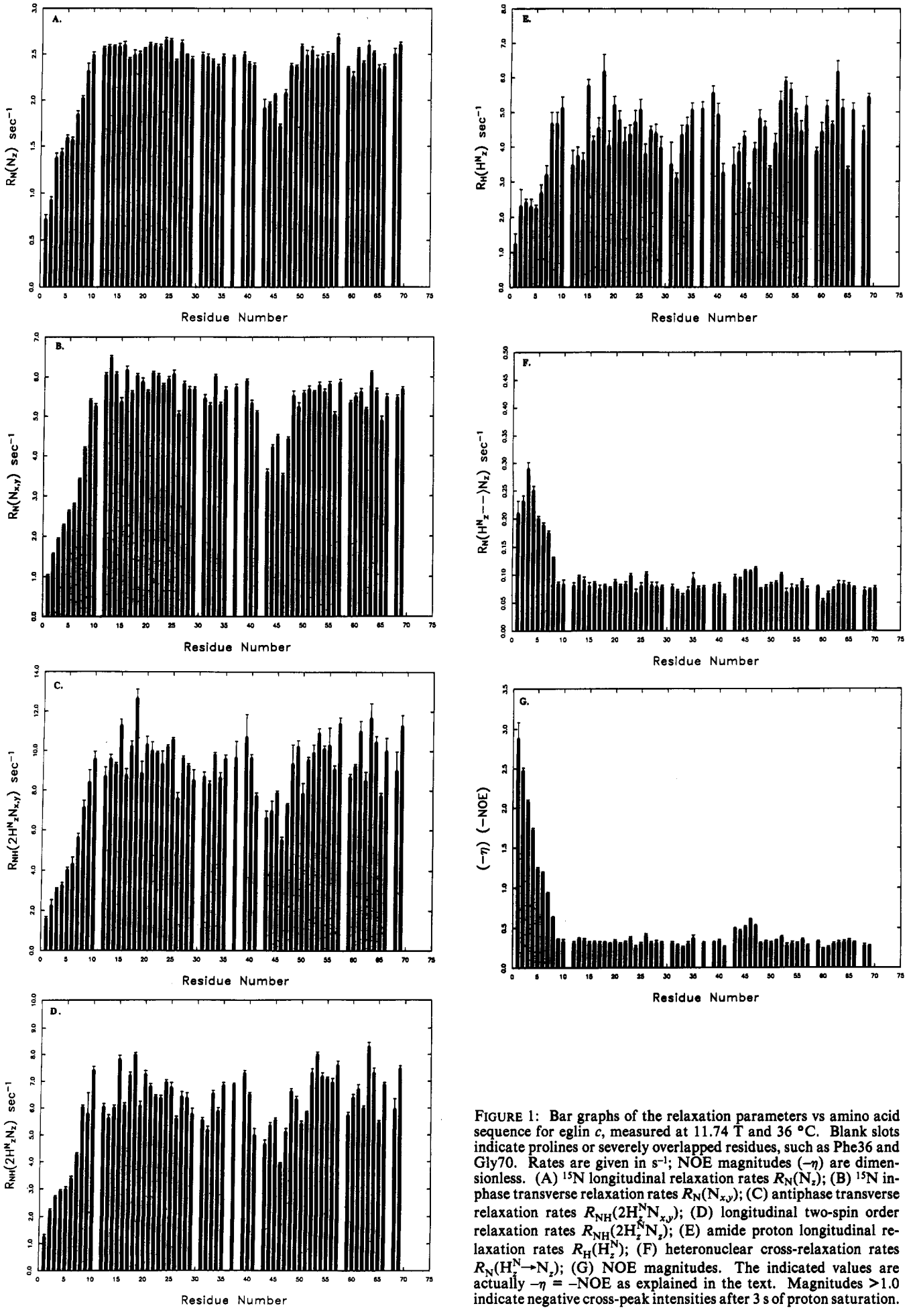


FIGURE 1: Bar graphs of the relaxation parameters vs amino acid sequence for eglin *c*, measured at 11.74 T and 36 °C. Blank slots indicate prolines or severely overlapped residues, such as Phe36 and Gly70. Rates are given in $s^{-1}$; NOE magnitudes ($-\eta$) are dimensionless. (A) $^{15}N$ longitudinal relaxation rates $R_N(N_z)$; (B) $^{15}N$ in-phase transverse relaxation rates $R_N(N_{x,y})$; (C) antiphase transverse relaxation rates $R_{NH}(2H^N_zN_{x,y})$; (D) longitudinal two-spin order relaxation rates $R_{NH}(2H^N_zN_z)$; (E) amide proton longitudinal relaxation rates $R_H(H^N_z)$; (F) heteronuclear cross-relaxation rates $R_N(H^N_z \rightarrow N_z)$; (G) NOE magnitudes. The indicated values are actually $-\eta = -NOE$ as explained in the text. Magnitudes >1.0 indicate negative cross-peak intensities after 3 s of proton saturation.

Phe36 and Gly70 and Tyr56 and Val43. The overlap is more severe for the former pair, which constitutes essentially a single cross-peak in the 2D $^1H$–$^{15}N$ correlated spectra. As a result, reliable values of the relaxation parameters for the individual residues cannot be obtained. Estimates for the Phe36 and Gly70 relaxation parameters derived from the single aggregate peak are listed in the supplementary material. They are not shown in the bar graphs of Figure 1.

Figure 1 correlates the six relaxation parameters with the protein sequence. The ranges of the relaxation rates (in $s^{-1}$) were as follows: $0.72 < R_N(N_z) < 2.68$, $1.02 < R_N(N_{x,y}) < 6.49$, $1.58 < R_{NH}(2H_z^N N_{x,y}) < 12.65$, $1.25 < R_{NH}(2H_z^N N_z) < 8.29$, $1.23 < R_H(H_z^N) < 6.18$, and $0.001 < R_N(H_z^N \rightarrow N_z) < 0.022$. In what follows, it will be convenient to refer to all relaxation rates excluding the cross-relaxation rate $[R_N(H_z^N \rightarrow N_z)]$ as direct relaxation rates. The NOEs, as defined in eq 8, ranged from –0.23 to –2.88. This means that the cross-peak intensities ranged from 77 to –188% of the equilibrium intensity, as a result of the Overhauser effect induced by proton saturation. Figure 1 shows noticeably different relaxation behavior for the eight N-terminal residues Thr1–Lys8 and an internal stretch of residues including Val43–Leu47. If we discount these residues, then the relaxation parameters for the remaining 51 NH vectors are much more uniform. These remaining residues constitute the protein core. The average values and uncertainties for the core relaxation rates are $R_N(N_z) = 2.48$, $R_N(N_{x,y}) = 5.61$, $R_{NH}(2H_z^N N_{x,y}) = 9.59$, $R_{NH}(2H_z^N N_z) = 6.45$, $R_H(H_z^N) = 4.62$, and $R_N(H_z^N \rightarrow N_z) = 0.080\ s^{-1}$. The average uncertainties ($\pm\delta$) for these rates are as follows: $\delta R_N(N_z) = 0.05$, $\delta R_N(N_{x,y}) = 0.08$, $\delta R_{NH}(2H_z^N N_{x,y}) = 0.42$, $\delta R_{NH}(2H_z^N N_z) = 0.15$, $\delta R_H(H_z^N) = 0.27$, and $\delta R_N(H_z^N \rightarrow N_z) = 0.005\ s^{-1}$. The two-spin relaxation rates $[R_{NH}(2H_z^N N_{x,y})$ and $R_{NH}(2H_z^N N_z)]$ exceed their one-spin counterparts $[R_N(N_{x,y})$ and $R_N(N_z)]$ by roughly $4.0\ s^{-1}$, as a consequence of the longitudinal relaxation of the attached amide proton ($H^N$). The average NOE value is –0.32, and the average uncertainty is $\delta$NOE = 0.02. Thus, the cross-peak intensities after proton saturation were typically reduced to ≈68% of that observed without the saturation.

The NH vectors of the N terminus and the internal segment Val43–Leu47 are distinguished by much smaller direct relaxation rates. The cross-relaxation rates are significantly larger for the N terminus but not for residues Val43–Leu47. The heteronuclear NOEs are much stronger (more negative) for both regions. Figure 1 plots $-\eta$ and thus shows the magnitudes of the NOEs. The first six residues have NOE magnitudes >1.0; this corresponds to negative cross-peak intensities after proton saturation. The magnitudes decrease in a monotonic fashion until a value similar to the quoted average of 0.32 is reached at Ser9. In an analogous fashion, the direct relaxation rates increase progressively along the N terminus and reach the above quoted averages at Ser9. In all cases, Thr1 has the smallest direct relaxation rates, with values which are only 15–30% of the core averages. As noted above, the N terminus of expressed eglin c is acetylated in a posttranslational event (Märki et al., 1985). Thus, Thr1 has a single amide NH vector instead of three, and therefore the analysis of the relaxation data remains the same. The relaxation parameters for residues in the segment Val43–Leu47 cause a "dip" in the middle of the bar graphs. These residues are a subset of the proteinase binding loop of eglin c which includes residues Ser41–Arg48 (McPhalen et al., 1985; Bode et al., 1986, 1987; Hyberts & Wagner, 1990). While the values of these parameters deviate significantly from the average values, the difference is not as severe as in case of the N-terminal residues. The most conspicuous residue is Asp46, which has relaxation properties similar to those of the N-terminal residues Leu7 and Lys8. The deviant relaxation behavior of the N terminus and proteinase binding loop, while still visible, is less easily distinguished in the $R_{NH}(2H_z^N N_{x,y})$, $R_{NH}(2H_z^N N_z)$, and $R_H(H_z^N)$ values. This is most likely due to the combined effects of larger errors associated with these measurements and an intrinsically greater variability in the amide proton longitudinal relaxation rate. NOE values for the side chain $\epsilon$ NH vectors of Arg22, Arg48, Arg51, and Arg53 have also been measured. These values are $-1.330 \pm 0.018$, $-2.156 \pm 0.004$, $-0.353 \pm 0.018$, and $-0.591 \pm 0.012$ for the side chains of Arg22, Arg48, Arg51, and Arg53, respectively. Measurements for the full set of relaxation parameters have not been completed for these side-chain NH vectors, due to complications from off-resonance effects in the spin-locked $R_N(N_{x,y})$ and $R_{NH}(2H_z^N N_{x,y})$ experiments; this work is continuing. It is interesting to note that the NOE value for Arg51$\epsilon$ is similar to the protein core average, whereas those of Arg22$\epsilon$ and Arg48$\epsilon$ are more similar to that of the N terminus. Arg53$\epsilon$ has a value close to that of the amide NH vector of Asp46. In the crystal structure of the complex eglin c with subtilisin Carlsberg, the side chains of Arg51 and Arg53 are involved in hydrogen bonds with the proteinase binding loop (McPhalen et al., 1985; Bode et al., 1986, 1987; McPhalen & James, 1988). These hydrogen bonds help stabilize the conformation of the binding loop. The hydrogen bonding may restrict the orientational freedom of the Arg51$\epsilon$ and Arg53$\epsilon$ NH vectors and explain why their NOE values more resemble those of the protein core.

*Spectral Density Values for Eglin c.* Use of eqs 13–17 directly yields the NH spectra density values, $J(\omega)$, at 0, $\omega_N$, $\omega_{H^N} + \omega_N$, $\omega_{H^N}$, and $\omega_{H^N} - \omega_N$ (0, 50.68, 449.46, 500.14, and 550.82 MHz, respectively). Listings of the $J(\omega)$ values and estimated uncertainties are given in the supplementary material. The estimated uncertainties were derived from the aforementioned 500 Monte Carlo simulations. Synthetic spectral density values were calculated from the ensemble of simulated relaxation data sets, and the resulting standard deviations were taken as the uncertainties.

Flexibility along the protein backbone can be characterized by correlating the spectral density values with the protein sequence. The backbone of eglin c can be seen in the bundle of structures shown in the stereo pair of Figure 2. The figure is derived from the NMR structure determinations for eglin c (Hyberts & Wagner, 1990; Hyberts et al., 1992). The proteinase binding loop is at the top of the figure. The secondary structural elements constituting the protein core can be seen underneath.

Figure 3 plots the five spectral density values vs sequence. As foreshadowed by the relaxation rates, the spectral density values for the 51 NH vectors of the protein core are fairly uniform. The uniformity indicates that the bulk of the NH vectors have very similar motional properties; significant deviations from this uniformity indicate increased internal mobility of the relevant NH vectors. Additionally, the uniformity suggests that the assumption of isotropic overall rotational diffusion for the protein is reasonable. The average $J(\omega)$ values for the core NH vectors are $J(0) = 1.33$ ns/rad, $J(\omega_N) = 0.46$ ns/rad, $J(\omega_{H^N}+\omega_N) = 0.023$ ns/rad, $J(\omega_{H^N}) = 0.045$ ns/rad, and $J(\omega_{H^N}-\omega_N) = 0.076$ ns/rad. The average uncertainties ($\pm\delta$) for the $J(\omega)$ values are as follows: $\delta J(0) = 0.07$ ns/rad, $\delta J(\omega_N) = 0.03$ ns/rad, $\delta J(\omega_{H^N}+\omega_N) = 0.011$ ns/rad, $\delta J(\omega_{H^N}) = 0.060$ ns/rad, and $\delta J(\omega_{H^N}-\omega_N) = 0.063$ ns/rad. When all quantifiable NH vectors are considered,the

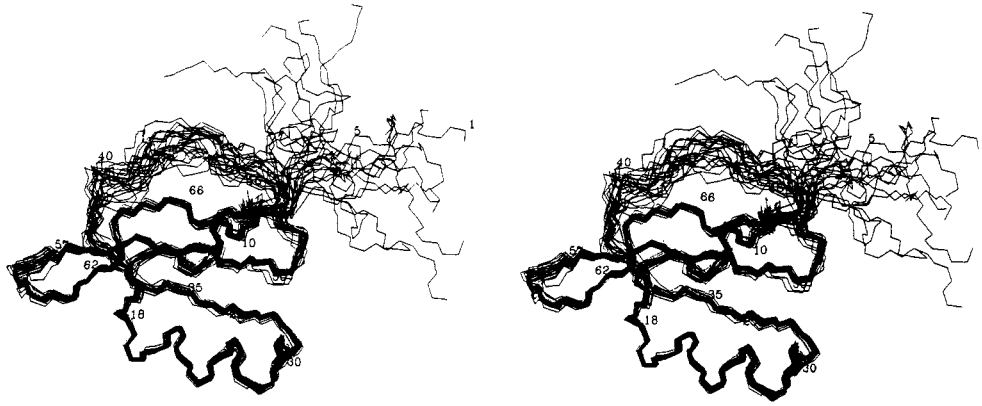

FIGURE 2: Backbone traces of eglin *c* based on NMR solution structure determinations (Hyberts & Wagner, 1990; Hyberts et al., 1992). The proteinase binding loop is positioned at the top of the figure, and the N terminus is at the upper right.

ranges of the $J(\omega)$ values are $0.16 < J(0) < 1.63$ ns/rad, $0.08 < J(\omega_N) < 0.54$ ns/rad, $-0.003 < J(\omega_{H^N}+\omega_N) < 0.053$ ns/rad, $-0.097 < J(\omega_{H^N}) < 0.141$ ns/rad, and $-0.073 < J(\omega_{H^N}-\omega_N) < 0.197$ ns/rad. The appearance of the unphysical "negative" $J(\omega)$ values at the higher frequencies is a consequence of their apparently smaller values ($\approx$0.01–0.1 ns/rad) and the larger random errors associated with them. Typically, the estimated errors are on the order of these $J(\omega)$ values themselves. This is especially true for the $J(\omega_{H^N})$ and $J(\omega_{H^N}-\omega_N)$. Figure 3 clearly shows that the $J(\omega_{H^N})$ and $J(\omega_{H^N}-\omega_N)$ values are much more sensitive to statistical fluctuations in the relaxation data. This sensitivity can be seen from eqs 14 and 16, which show that $J(\omega_{H^N})$ and $J(\omega_{H^N}-\omega_N)$ depend on differences of relaxation rates that have very similar values.

For many residues, $J(\omega)$ appears to increase slightly from $J(\omega_{H^N}+\omega_N)$ at 449.45 MHz to $J(\omega_{H^N}-\omega_N)$ at 550.82 MHz. While such increases in the spectral density function are possible in principle, they are forbidden by current popular models of motion. The Lipari and Szabo model function $J(\omega)_{ls}$ in eq 22 is an example. Certain systematic errors in the rate measurements may contribute to this increase, and this will be discussed in what follows. Large overestimations of $J(\omega_{H^N})$ and $J(\omega_{H^N}-\omega_N)$ as a result of random errors in the relaxation rates may also give the illusion of an increase.

Figure 3 shows that the NH vectors of the eight N-terminal residues undergo the most rapid motions compared to the rest of the protein backbone. This is evidenced most clearly by the smaller $J(0)$ values. As stated, the smaller $J(0)$ values imply that the NH vectors of these residues reorient on a characteristically faster time scale than the core residues. Additionally, the smaller values indicate that the $J(\omega)$ shapes are significantly broader than those of the core. The most extreme example is Thr1, which has a $J(0)$ value of 0.16 $\pm$ 0.03 ns/rad; this represents only about 10% of the core average value. Similarly, the $J(\omega_N)$ values for the N terminus are smaller than the protein average as well. In contrast, the spectral density values at the higher frequencies are comparable to the core averages. We note that the $J(0)$ and $J(\omega_N)$ values display a steady increase from Thr1 to Lys8. Values typical of the protein core are achieved at Ser9. This suggests a progressive constraining of the NH vectors, until motions typical of the protein core are reached at Ser9. It is interesting to note the first seven residues do not appear in the crystal structure of eglin *c* in complex with subtilisin Carlsberg (McPhalen et al., 1985; McPhalen & James, 1987, 1988). The $J(\omega)$ data here suggest that this absence is due to a progressive increase of rapid motions from Lys8 to Thr1. An analogous increase is not observed for the corresponding C terminus. This is a consequence of the fact that the C-terminal residues are involved in an extensive hydrogen bond network (Bode et al., 1986; Hyberts & Wagner, 1990; Hyberts et al., 1992; Heinz et al., 1992).

Significant internal motions are also indicated for the binding loop NH vectors of residues Val43–Leu47, which form the proteinase binding loop. However, these vectors are not as flexible as those in the N terminus. Their increased mobility is evidenced primarily by the decrease of the $J(0)$ and $J(\omega_N)$ values after Ser41 and the rather sudden return to the core values at Arg48. Thus, these binding loop residues define an isolated region of increased flexibility in the midst of the protein sequence. Unfortunately, position 42 is a proline, and the spectral density values of Val43 are less precise due to cross-peak overlap with Tyr56. Therefore, it cannot be clearly defined how abrupt the transition is from typical core $J(\omega)$ values down to the binding loop values. The $P_1'$ residue Asp46 appears to have the most mobile NH vector in this region with a $J(0)$ of 0.76 $\pm$ 0.03 ns/rad. This value represents $\approx$57% of the core average and is almost identical to that of Lys8. Therefore, the binding loop residues appear to possess a motional freedom intermediate between those of the N terminus and the protein core.

To help characterize the overall shape of $J(\omega)$, one can compare the ratios $J(\omega)/J(0)$ for different residues. All NH vectors have $J(0)$ as the largest samplings, and therefore all of the normalized values are $\leq$1.0. For the 51 core NH residues, the $J(\omega_N)$ values are typically 35% of $J(0)$. While this represents a substantial decrease in intensity, $J(\omega_N)$ is still significant in comparison to $J(0)$. However, the $J(\omega_{H^N}+\omega_N)$ values represent only about 2% of the $J(0)$ values. The highest frequency spectral density values $J(\omega_{H^N})$ and $J(\omega_{H^N}-\omega_N)$ are also quite small relative to $J(0)$ ($\approx$3–10%), although they display a much greater dispersion among the residues. This simply reflects the larger random fluctuations in the data discussed above. Therefore, despite the lack of precision in the absolute values of $J(\omega_{H^N})$ and $J(\omega_{H^N}-\omega_N)$, they are clearly much smaller than either $J(0)$ and $J(\omega_N)$ for the majority of residues. In contrast, the relative contributions of the high-frequency $J(\omega)$ values are more significant for the N-terminal residues. The more even weighting of $J(\omega)$ values is consistent with requirement that $J(\omega)$ enclose a constant area; therefore, smaller $J(\omega)$ values observed at lower frequency (0, 50.68 MHz) are paid for by contributions at higher frequencies (449.46, 500.14, 550.82 MHz). This result is also consistent with the small $J(0)$ values described above, which demands a broader shape for $J(\omega)$. The broader frequency range shows that the N-terminal NH vector fluctuations contain a greater amount of higher frequency motions. The relative contributions of the higher frequency

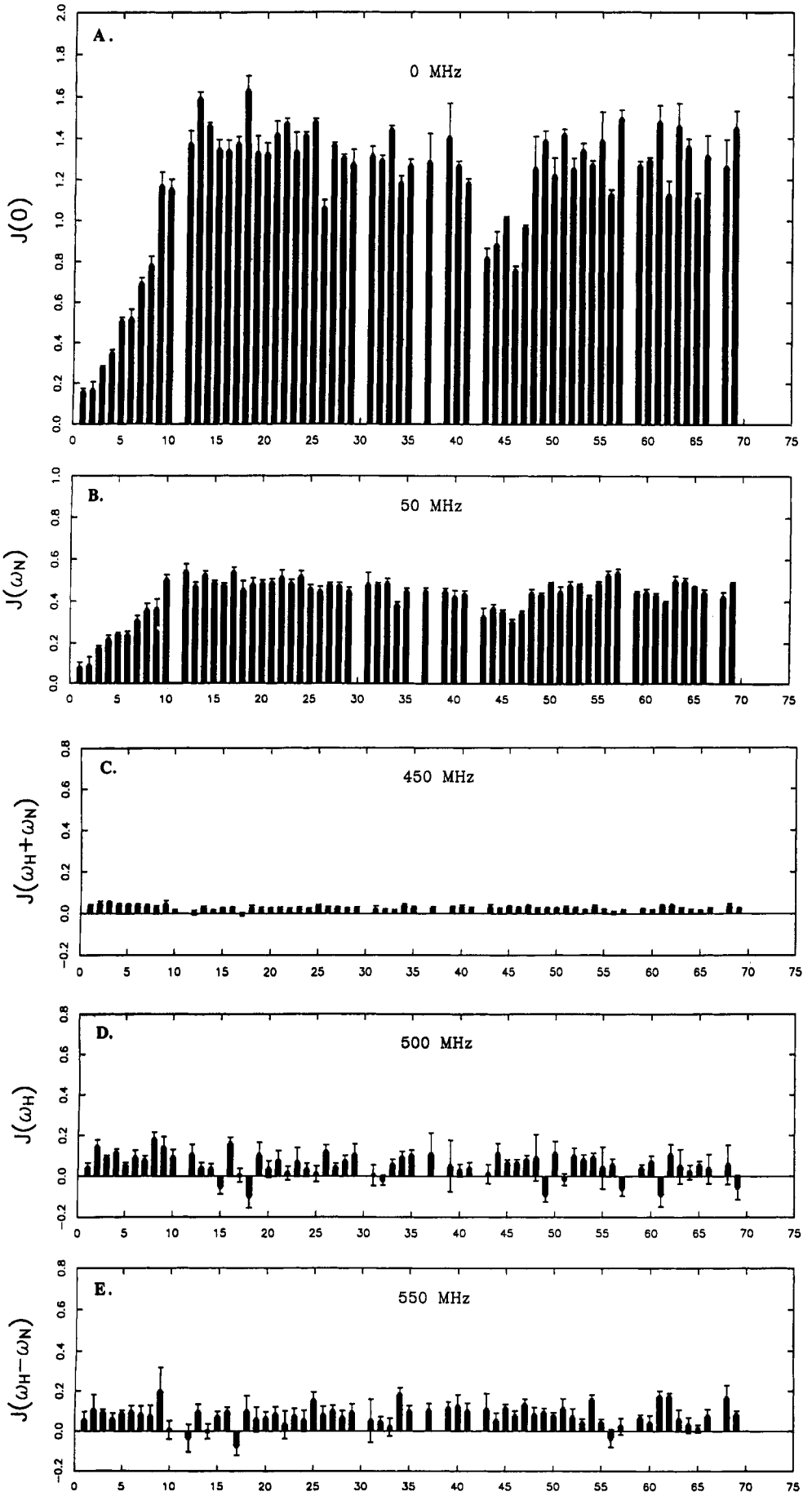


FIGURE 3: Five spectral density values, (A) $J(0)$, (B) $J(\omega_N)$, (C) $J(\omega_{H^N}+\omega_N)$, (D) $J(\omega_{H^N})$, and (E) $J(\omega_{H^N}-\omega_N)$, vs amino acid sequence for eglin *c*. The sampled angular frequencies correspond to approximately 0, 50, 450, 500, and 550 MHz, respectively. The plots are made to the same scale, and $J(\omega)$ values are quoted in nanoseconds per radian. Residue numbers are indicated on the horizontal axes. Errors were estimated using Monte Carlo simulations described in the text. Blank slots indicate prolines or severely overlapped residues, such as Phe36 and Gly70. The $J(0)$ values (A) can be interpreted as being proportional to generalized, local correlation times as discussed in the text.

Table I: Average Spectral Density Values for Different Structural Groups in Eglin $c$[a]

| structural unit[b] | $J(0)$ | $J(\omega_N)$ | $J(\omega_{H^N}+\omega_N)$ | $J(\omega_{H^N})$ | $J(\omega_{H^N}-\omega_N)$ |
|---|---|---|---|---|---|
| antiparallel $\beta$-sheet (15) | 1.30 (0.20) | 0.45 (0.05) | 0.025 (0.012) | 0.043 (0.083) | 0.086 (0.072) |
| parallel $\beta$-sheet (12) | 1.30 (0.10) | 0.46 (0.04) | 0.024 (0.010) | 0.067 (0.046) | 0.083 (0.059) |
| $\alpha$-helix (12) | 1.37 (0.13) | 0.48 (0.02) | 0.024 (0.005) | 0.051 (0.056) | 0.078 (0.030) |
| turns (6) | 1.38 (0.13) | 0.50 (0.02) | 0.017 (0.009) | 0.065 (0.067) | 0.038 (0.050) |
| loop(9) | 1.06 (0.21) | 0.38 (0.05) | 0.028 (0.005) | 0.061 (0.030) | 0.099 (0.025) |
| N terminus (8) | 0.04 (0.18) | 0.19 (0.08) | 0.042 (0.006) | 0.089 (0.033) | 0.082 (0.1018) |

[a] All values are reported in nanoseconds per radian. [b] The number of residues averaged over is indicated in parentheses next to the structural type. The standard deviation of the values for the various structural groups are in parentheses next to the average values.

$J(\omega)$ values are slightly greater for the proteinase bindingloop residues. However, the effect is not nearly as dramatic as in the case of the N terminus. Thus, while the higher frequency spectral density values may be very small, they are still useful since their comparison with $J(0)$ can be a key indicator of significant internal mobility.

Table I lists the average $J(\omega)$ values for different structural units in eglin $c$. The numbers in parentheses are the standard deviations of the $J(\omega)$ values for the particular structural motif. Apparently, NH vectors involved in different elements of regular secondary structure do not show major differences in the $J(\omega)$ values. There appears to be a slightly higher average for $J(0)$ values in the $\alpha$-helix (Val18–Tyr29) and for residues in tight turns (Ser9–Lys16). Essentially no differences are exhibited at the higher frequency values. The lower frequency spectral density values, $J(0)$ and $J(\omega_N)$, more obviously distinguish between those residues involved in secondary structure and those that are not. The latter class are represented by the N-terminal and proteinase binding loop NH vectors. In the structural studies of eglin $c$, the backbone along these regions is the least well-defined. This will be discussed more fully in the following section. Somewhat smaller $J(0)$ values are also seen for Thr26, Tyr56, Val62, and His65. In the case of Tyr56, this is likely due to artifacts in the rate analysis due to overlap with Val43 and with Ser5 to a lesser extent. The smaller $J(0)$ values for Thr26, Val62, and His65 are less easily rationalized. For example, both Thr26 and Val62 are involved in regular secondary structure. Thr26 is part of an $\alpha$-helix whose NH vectors typically show the least motional freedom, and Val62 is part of $\beta$-strand at the C terminus. The smaller $J(0)$ value for His65 may be a result of its location in a $\beta$-bulge. It is interesting to ascertain whether $J(0)$ correlates with the hydrogen bonding state of the NH vectors. One might expect that NH vectors not involved in intramolecular hydrogen bonds would experience more mobility and, hence, have smaller $J(0)$ values. Here, the hydrogen bonding capacities of the NH vectors are taken from the crystal structure data of eglin $c$ in complex with subtilisin Carlsberg (Bode et al., 1986). NH vector that are likely hydrogen bond donors have an average $J(0)$ value of 1.35 ns/rad, while those that are not have an average $J(0)$ of 1.31 ns/rad. In the latter class, we have excluded those NH vectors that are in the N terminus and in the proteinase binding loop. Thus, the non-hydrogen bonding NH vectors have an average $J(0)$ that is 0.04 ns/rad less than that of the hydrogen bonding vectors. However, given that the estimated experimental error of $J(0)$ is 0.07 ns/rad, this difference cannot be interpreted as significant.

Figure 4 plots the experimental $J(\omega)$ vs $\omega$ for four representative residues including Phe3, Arg22, Asp46, and Arg53. Arg22 is part of an $\alpha$-helix that stretches from Val18 to Tyr29, while Arg53 is part of a $\beta$-strand which includes residues Asn50–Tyr56. The NH vectors of these residues have a $J(\omega)$ distribution typical of the protein core. Their spectral densities are clearly biased toward lower frequencies, indicating less mobility. The higher frequency components make almost negligible contributions, especially in the case of Arg22. As the NH vector under study becomes more mobile, the $J(\omega)$ values suggest progressively flatter distributions. This is seen in the progression from Arg22 to Asp46 and then to Phe3. The highly mobile Phe3 appears to have an almost flat distribution for $J(\omega)$. Thus, as stated earlier, the increased mobility of the NH vector amounts to a "stretching out" of the spectral density function while insisting on a constant area. From Figure 4, it will clearly be useful to perform relaxation experiments that give information about $J(\omega)$ in frequencies between 50.68 and 449.46 MHz.

*Model-Free Parameters.* In this study, only $R_N(N_z)$ and $R_N(N_{x,y})$ rates and the NOE data at 500 MHz were used to obtain the model-free parameters described by Lipari and Szabo (1982a,b). The fitting protocol was similar to those established in previous studies of protein $^{15}N$ or natural abundance $^{13}C$ relaxation (Kay et al., 1989; Clore et al., 1990a,b; Palmer et al., 1991a,b). As shown by Kay et al. (1989), an initial estimate of the overall molecular tumbling time $\tau_m$ can be obtained using the ratios of $R_N(N_{x,y})$ over $R_N(N_z)$. In the limit of fast internal motions ($\tau_e \ll \tau_m$), this ratio depends only on $\tau_m$. If only the core residues are considered, the average ratio is 2.29 with a standard deviation of 0.10. The N-terminal residues have ratios ranging from 1.41 to 2.10, whereas the binding loop residues have ratios from 1.90 to 2.18. Using the core averaged value, an initial estimate of 4.13 ± 0.05 ns was obtained for $\tau_m$.

The residue-specific motional parameters $S^2$ and $\tau_e$ were varied for each NH vector with $\tau_m$ held fixed to minimize the error function.

$$E = \sum\left(\frac{R_{\text{obs } i} - R_{\text{modelfree } i}}{\sigma_i}\right)^2 \qquad (25)$$

$E$ is simply the sum of the squared residuals over all NH vectors. The rate uncertainties $\sigma_i$ were taken directly from the aforementioned Monte Carlo simulations. Minimization of $E$ involved using a Levenburg–Marquardt algorithm with the constraints that $0 \le S^2 \le 1.0$ and $\tau_e > 0$. After a given minimization of $E$, $\tau_m$ was stepped and $S^2$ and $\tau_e$ were reoptimized for all NH vectors. In this fashion, a grid search in $\tau_m$ was performed until a local minimum in $E$ was found (Dellwo & Wand, 1989). Estimations for the minimum error of the model-free parameters were obtained by performing the fitting protocol on an ensemble of Monte Carlo simulated data sets (Palmer et al., 1991a,b). The ensemble was generated by using relaxation rates predicted by $J(\omega)_{ls}$ (see eq 22) as the means of the Gaussian distributions and the $\sigma_i$ above as the corresponding widths. Using these methods, an overall correlation time of 4.15 ± 0.05 ns was found. The resulting values of the order parameters $S^2$ and the effective internal correlation times $\tau_e$ for each residue are listed in Table II.

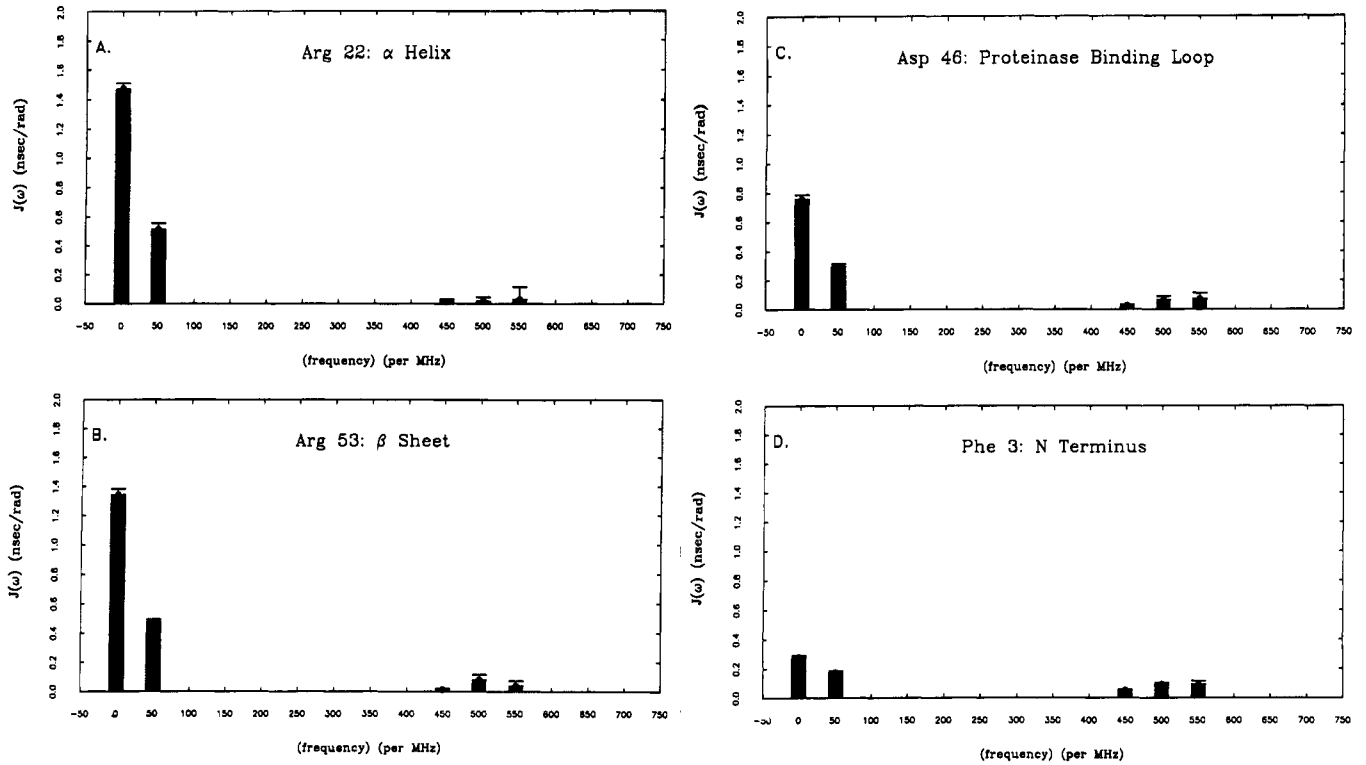


FIGURE 4: Spectral density profiles of $J(\omega)$ vs $[\omega/2\pi]$ for representative residues in eglin *c* including (A) Arg22, (B) Arg53, (C) Asp46, and (D) Phe3. All plots are made to the same scale, and $J(\omega)$ is given in nanoseconds per radian. Arg22 and Arg53 are involved in regular secondary structure. The implied flat distribution of Phe3 is a characteristic feature of high internal flexibility. Phe3 is the N terminus and is not involved in secondary structure. Asp46 has a distribution between that of Arg22 (or Arg53) and Phe3.

Table II: Eglin *c* Model-Free Parameters:[a] 500 MHz, pH 3.0, $T$ = 36 °C, 3.8 mM

| residue[b] | $S^2$ | $\tau_e$ (ps) | residue[b] | $S^2$ | $\tau_e$ (ps) |
|---|---|---|---|---|---|
| Thr1 | 0.08 ± 0.01 | 102.8 ± 1.9 | Tyr35 | 0.83 ± 0.02 | <25 |
| Glu2 | 0.16 ± 0.01 | 104.2 ± 2.8 | Phe36* | 0.81 ± 0.01 | <25 |
| Phe3 | 0.18 ± 0.01 | 183.7 ± 1.5 | Leu37 | 0.83 ± 0.01 | <25 |
| Gly4 | 0.25 ± 0.01 | 171.7 ± 3.6 | Glu39 | 0.86 ± 0.01 | <25 |
| Ser5 | 0.32 ± 0.01 | 142.1 ± 3.2 | Gly40 | 0.78 ± 0.01 | 42.4 ± 20.1 |
| Glu6 | 0.36 ± 0.01 | 121.6 ± 2.6 | Ser41 | 0.75 ± 0.01 | 37.2 ± 17.4 |
| Leu7 | 0.46 ± 0.01 | 112.1 ± 0.3 | Val43* | 0.52 ± 0.01 | 43.8 ± 0.8 |
| Lys8 | 0.60 ± 0.01 | 81.8 ± 0.3 | Thr44 | 0.61 ± 0.01 | 51.1 ± 7.4 |
| Ser9 | 0.79 ± 0.01 | 32.1 ± 3.8 | Leu45 | 0.65 ± 0.01 | 65.6 ± 10.5 |
| Phe10 | 0.76 ± 0.02 | 155.1 ± 54.3 | Asp46 | 0.51 ± 0.01 | 52.4 ± 1.0 |
| Glu12 | 0.89 ± 0.02 | <25 | Leu47 | 0.64 ± 0.01 | 66.5 ± 1.4 |
| Val13 | 0.92 ± 0.01 | <25 | Arg48 | 0.79 ± 0.01 | <25 |
| Val14 | 0.89 ± 0.02 | <25 | Tyr49 | 0.78 ± 0.01 | 33.6 ± 13.7 |
| Gly15 | 0.81 ± 0.01 | 120.8 ± 35.8 | Asn50 | 0.83 ± 0.01 | 68.5 ± 23.2 |
| Lys16 | 0.89 ± 0.01 | <25 | Arg51 | 0.83 ± 0.01 | 37.3 ± 7.3 |
| Thr17 | 0.82 ± 0.02 | <25 | Val52 | 0.82 ± 0.01 | 78.8 ± 10.2 |
| Val18 | 0.87 ± 0.01 | <25 | Arg53 | 0.85 ± 0.01 | <25 |
| Asp19 | 0.84 ± 0.01 | <25 | Val54 | 0.82 ± 0.01 | <25 |
| Gln20 | 0.82 ± 0.01 | 94.7 ± 48.2 | Phe55 | 0.85 ± 0.01 | <25 |
| Ala21 | 0.89 ± 0.01 | <25 | Tyr56* | 0.77 ± 0.01 | 130.6 ± 27.6 |
| Arg22 | 0.88 ± 0.01 | <25 | Asn57 | 0.87 ± 0.01 | 48.1 ± 28.5 |
| Glu23 | 0.84 ± 0.01 | 75.0 ± 28.5 | Gly59 | 0.78 ± 0.01 | 25.4 ± 7.1 |
| Tyr24 | 0.88 ± 0.01 | <25 | Thr60 | 0.80 ± 0.01 | <25 |
| Phe25 | 0.89 ± 0.01 | <25 | Asn61 | 0.85 ± 0.01 | <25 |
| Thr26 | 0.76 ± 0.01 | 97.7 ± 14.6 | Val62 | 0.76 ± 0.01 | 64.3 ± 24.4 |
| Leu27 | 0.85 ± 0.01 | 57.6 ± 37.7 | Val63 | 0.90 ± 0.02 | <25 |
| His28 | 0.83 ± 0.02 | <25 | Asn64 | 0.83 ± 0.01 | 48.0 ± 43.4 |
| Tyr29 | 0.83 ± 0.01 | <25 | His65 | 0.74 ± 0.01 | 46.1 ± 7.2 |
| Gln31 | 0.81 ± 0.01 | 50.3 ± 21.8 | Val66 | 0.79 ± 0.01 | <25 |
| Tyr32 | 0.79 ± 0.01 | 29.9 ± 10.9 | His68 | 0.81 ± 0.01 | 27.9 ± 15.6 |
| Asp33 | 0.89 ± 0.01 | <25 | Val69 | 0.85 ± 0.01 | <25 |
| Val34 | 0.78 ± 0.01 | <25 | Gly70* | 0.81 ± 0.01 | <25 |

[a] The overall molecular correlation time ($\tau_m$) is 4.15 ± .05 ns. [b] Asterisks indicate residues with significant cross-peak overlap in the spectra. Gly70 and Phe36 are essentially completely overlapped.

Figure 5 shows the order parameters $S^2$ as a function of residue number. The $S^2$ values ranged from a minimum of 0.08 to a maximum of 0.92. For the core NH vectors, the average order parameter is 0.83. This value is similar to those reported in other $^{15}N$ relaxation studies for residues involved in well-defined secondary structures (Kay et al., 1989; Clore et al., 1990a,b; Palmer et al., 1991a,b). If $S^2$ is further interpreted in the wobbling in a cone model (Woessner, 1962;

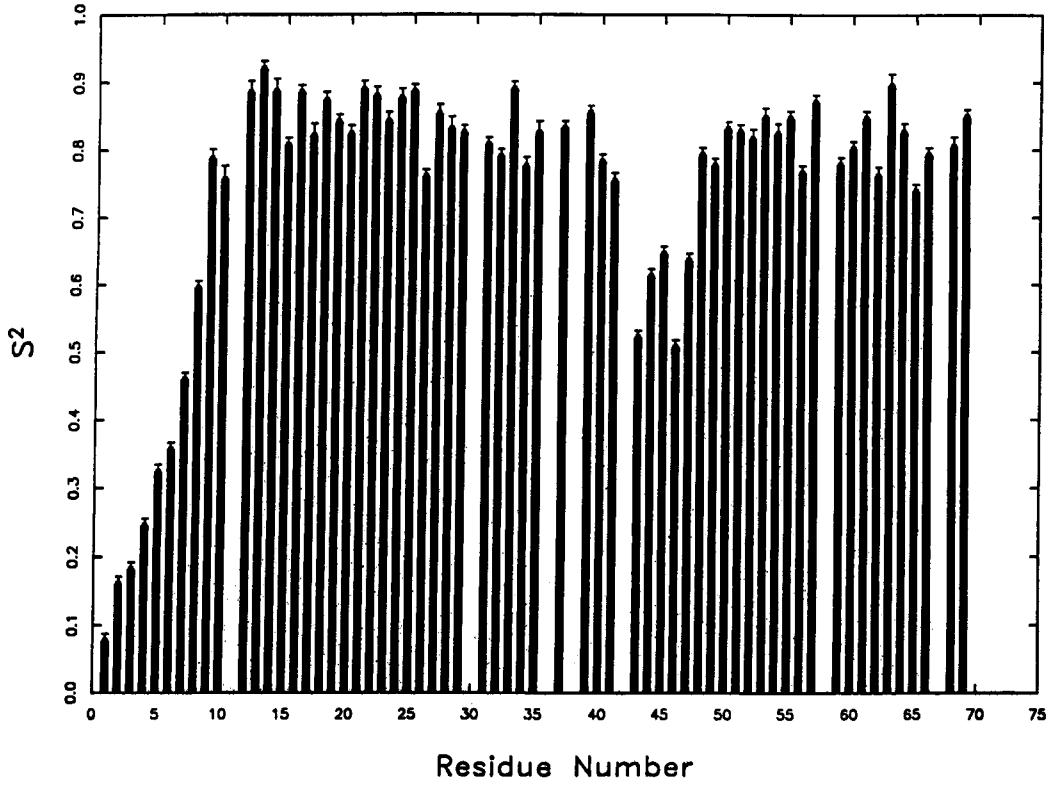


FIGURE 5: Generalized order parameters $S^2$ (Lipari & Szabo, 1982a,b) vs amino acid sequence for eglin *c*. The values are based only on the $R_N(N_z)$, $R_N(N_{x,y})$, and NOE data at 11.74 T (500 MHz). The average $S^2$ value of the core residues was 0.83. The minimum $S^2$ was 0.08 (Thr1), and the maximum $S^2$ was 0.92 (Val13). Effective correlation times for the internal motions were <25 ps for many residues and more substantial for the N terminus and proteinase binding loop.

Kinoshita et al., 1977; Richarz et al., 1980), then this value corresponds to a semiangle of ≈20°. The order parameters are lowest for the eight N-terminal residues. The smallest order parameter occurs for Thr1, which has $S^2 = 0.08 \pm 0.01$. Core average values for $S^2$ are obtained at Ser9. The proteinase binding loop residues also show lower order parameters. The values range from 0.51 ± 0.01 for Asp46 to 0.64 ± 0.01 for Leu45. As stated, lower $S^2$ values imply greater spatial freedom of the NH vector due to internal motions. The nearly zero value of Thr1 suggests that the internal motion of its NH vector allows almost complete spatial freedom. Typically, the largest order parameters are in the α-helix or in the turns consisting of residues Ser9–Lys16. The β-strand values are very similar, however. Thus, the generalized order parameters $S^2$ reveal the same regions of flexibility as those obtained from the experimental spectral density values. The estimated errors in the $S^2$ values derived from the Monte Carlo simulations gave values typically ≈0.01. However, this estimate appears overly optimistic and is probably due to an insufficient parameter sampling in the Monte Carlo simulations.

As discussed above, a physical interpretation of $\tau_e$ is difficult, since $\tau_e$ depends both on the amplitude and on the time scale of the internal motions. Additionally, the fitted $\tau_e$ values appear to be more sensitive to random errors in the relaxation measurements. What is clear is that different regimes of optimal $\tau_e$ values exist for different sets of NH vectors. In one regime, the $\tau_e$ values are estimated to be well below 25 ps; these residues are indicated in Table II. These cases occur for residues locked into secondary structure. Examples include residues Glu12–Val14, residues involved in the α-helix from Val18–Tyr29, and some residues involved in the β-strands. The small values correspond to the "extreme narrowing" limit for the internal motion, in which the characteristic time scales for the internal fluctuations are on the picosecond or below time scale. Larger values of $\tau_e$ are essential in fitting the relaxation data for the proteinase binding loop residues. The $\tau_e$ values range from 44 to 66 ps, and the corresponding errors are smaller. $\tau_e$ values in the range 100–200 ps are required for the N-terminal residues. Thus, the $\tau_e$ values suggest that the internal motions exist on different time scales for the N terminus and binding loop.

To determine whether the Lipari and Szabo formalism can adequately describe the relaxation data, the predicted relaxation parameters can be compared to the measured values. For most of the NH vectors, the $R_N(N_z)$ and $R_N(N_{x,y})$ are reproduced to within the limits of experimental error. The NOE discrepancies are typically larger, and for some residues, the discrepancies vastly exceed the estimated experimental errors. This is further described in the next section.

## DISCUSSION

The relaxation studies given here clearly indicate enhanced mobility for the NH vectors of the N-terminal and proteinase binding loop residues. The remaining NH vectors have significantly less mobility and have very similar motional properties. These results suggest a crude dynamic model of eglin *c* as being a well-structured, isotropically reorienting kernel supporting two more flexible segments.

The utility of the spectral density data is that it allows insight into the frequency content of the NH fluctuations. Equivalently, the relative contribution of motions on different time scales to the overall NH bond vector dynamics can be compared. The overall uniformity of the $J(\omega)$ values (excluding the aforementioned mobile regions) suggests that the backbone NH vectors undergo common motions with a frequency distribution typified by Arg22 and Arg53 in Figure 4. This distribution obviously includes the effects of overall molecular tumbling but also includes any common bond specific motions that are independent of the protein sequence. Of greater interest is the identification of the relevant frequency

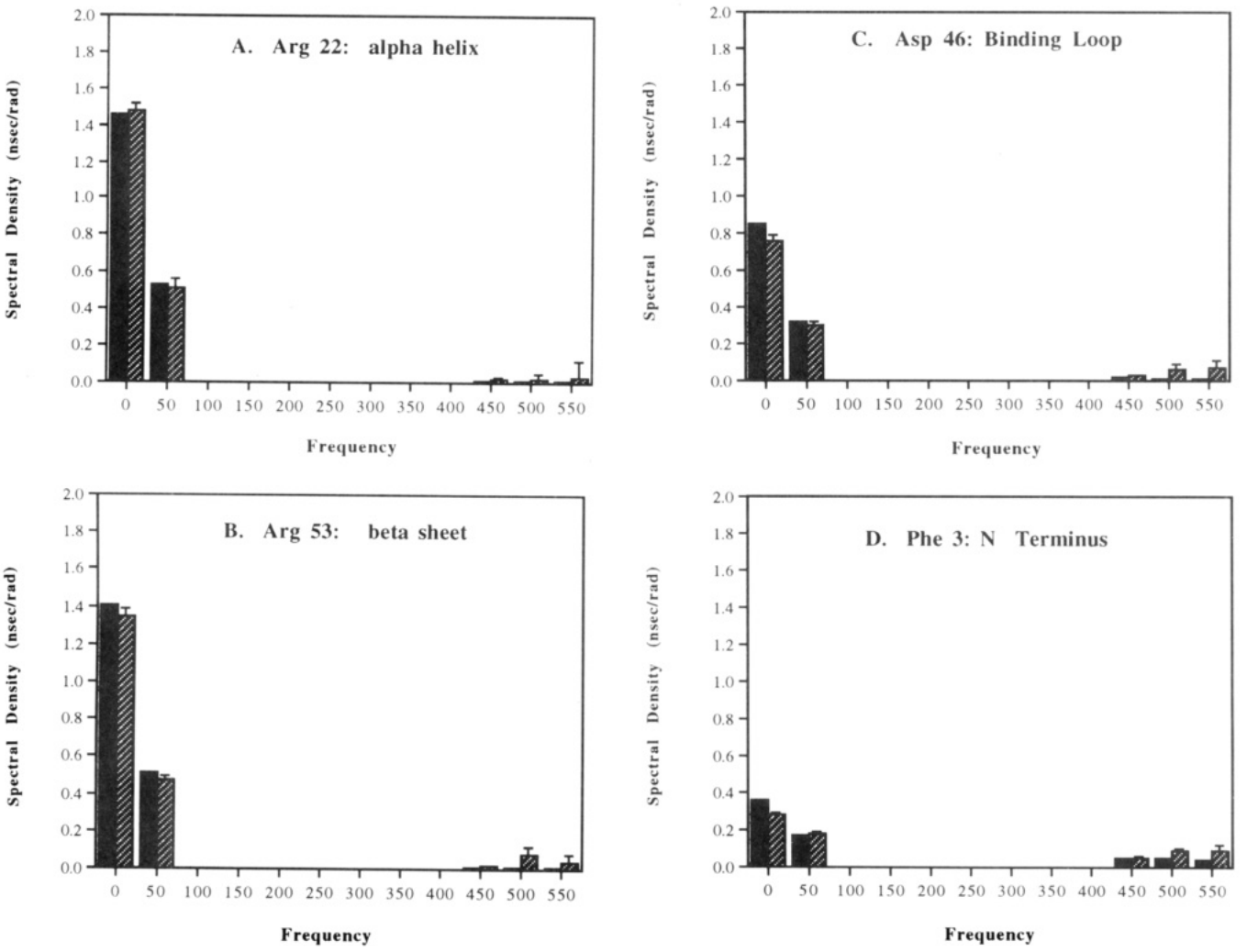


FIGURE 6: Comparison of $J(\omega)$ values from the original Lipari and Szabo (1982a,b) model-free formalism, expressed by $J(\omega)_{ls}$ in eq 22, and the direct mapping method for (A) Arg22, (B) Arg53, (C) Asp46, and (D) Phe3. The model-free values are given by the solid bars on the left, and the direct mapping values are given by the hatched bars on the right.

ranges for the internal motions exhibited by the N-terminal and proteinase binding loop residues. The bar graphs of Figure 3 reveal that $J(\omega_{H^N}+\omega_N)$, $J(\omega_{H^N})$, and $J(\omega_{H^N}-\omega_N)$ do not readily distinguish the N terminus and proteinase binding loop from the rest of the protein. Slightly larger $J(\omega_{H^N}+\omega_N)$ values are seen for the N terminus. However, the $J(\omega_{H^N})$ and $J(\omega_{H^N}-\omega_N)$ values are essentially uniform for all backbone NH vectors within experimental error. Thus, frequencies in the neighborhood of 500 MHz do not appear to be sensitive probes for the internal motion of the N terminus and binding loop. This lack of sensitivity in $J(\omega_{H^N}+\omega_N)$ and $J(\omega_{H^N}-\omega_N)$ may seem somewhat surprising when one considers the heteronuclear NOE data. In particular, the NOE magnitudes clearly reveal the mobile regions in Figure 1, and yet, the NOEs depend on $J(\omega_{H^N}+\omega_N)$ and $J(\omega_{H^N}-\omega_N)$. However, the NOEs depend both on $R_N(N_z)$ and on heteronuclear cross-relaxation rates $R_N(H_z^N \rightarrow N_z)$. Hence, the observed NOE variations depend not only on $J(\omega_{H^N}+\omega_N)$ and $J(\omega_{H^N}-\omega_N)$ but on $J(\omega_N)$ as well (see eqs 5 and 7). A more direct measure of the dynamical sensitivity of $J(\omega_{H^N}+\omega_N)$ and $J(\omega_{H^N}-\omega_N)$ is the cross-relaxation rates $R_N(H_z^N \rightarrow N_z)$ (Figure 1), which depend only on these samplings. The only notable variation in the $R_N(H_z^N \rightarrow N_z)$ values occurs for the first eight residues with cross-relaxation rates 1.5–2 times larger than the core average of 0.080 $s^{-1}$. In contrast, the existence of the mobile proteinase binding loop is fairly well masked. Thus, the larger NOEs seen for the binding loop are more a reflection of the smaller $R_N(N_z)$ values [i.e., smaller $J(\omega_N)$ values]. Collectively, the $J(\omega)$ data suggest that frequencies less than 450 MHz are much more characteristic of the internal motions. Both $J(0)$ and $J(\omega_N)$ exhibit significant decreases for the N-terminal and proteinase binding loop NH vectors. As stated, the inverse of $J(0)$ characterizes the effective bandwidth of frequencies for the NH vector motion. Accordingly, the decrease of $J(0)$ implies an increase of motions at some higher frequencies. This compensatory behavior may be distributed over a wide range of higher frequencies, and therefore mappings of $J(\omega)$ between 50 and 450 MHz would prove interesting. In general, a more dramatic variation of $J(\omega)$ vs $\omega$ may be seen if the sampling frequencies of $J(\omega)$ are altered. This simply means using different field strengths (e.g., 300 and 600 MHz) or a different spin system (e.g., $^{13}C-^{1}H$); the method of translating relaxation data into spectral density information is the same.

It is of interest to compare the $J(\omega)$ values obtained from experiment with those predicted by models of $J(\omega)$. Insertion of the optimized $\tau_m$, $S^2$, and $\tau_e$ values into eq 22 permits calculation of the expected spectral density values in the Lipari and Szabo approach, $J(\omega)_{ls}$. Figure 6 shows a juxtaposition of the five $J(\omega)$ values given by experiment and the Lipari and Szabo approach for residues Arg22, Arg53, Asp46, and Phe3. These four residues are representative for the $\alpha$-helix, the $\beta$-sheet, the binding loop, and the flexible N terminus, respectively. The experimental values are indicated by the hatched bars on the right. On average, the model-free approach predicts somewhat larger $J(0)$ and $J(\omega_N)$ values.

The average excesses are 0.06 and 0.03 ns/rad for $J(0)$ and $J(\omega_N)$, respectively. These excesses are not serious breaches since they are comparable to the average uncertainties of $J(0)$ and $J(\omega_N)$ (0.07 and 0.03 ns/rad, respectively). Conversely, the higher frequency values are systematically lower in the model-free formalism. On average, the $J(\omega_{H^N}+\omega_N)$, $J(\omega_{H^N})$, and $J(\omega_{H^N}-\omega_N)$ values are predicted to be 0.010, 0.040, and 0.067 ns/rad lower than the measured values, respectively. These discrepancies are a reflection of the conflicting interests between the aforementioned irregular behavior of the higher frequency $J(\omega)$ values obtained from experiment and the necessity of a monotonic decrease of the $J(\omega)_{ls}$ in eq 22. The magnitude of these discrepancies is not so severe, when one considers the estimated errors in the experimental values [0.011, 0.060, and 0.063 ns/rad for $J(\omega_{H^N}+\omega_N)$, $J(\omega_{H^N})$, and $J(\omega_{H^N}-\omega_N)$ respectively] and the characteristically small value of these spectral densities. NH vectors in the protein core show fairly good agreement between the two approaches, within the limits of experimental error. The plots of Arg22 and Arg53 in Figure 6 are examples of such cases. The experimental values for three higher frequency spectral densities are somewhat higher for Arg53. The more significant discrepancies occur for NH vectors belonging to the binding loop and N-terminal residues. These cases are illustrated by Asp46 and Phe3 in Figure 6. $J(\omega)_{ls}$ predicts substantially larger $J(0)$ values and smaller $J(\omega_{H^N}+\omega_N)$ and $J(\omega_{H^N})$ values for these residues. In some instances, the $J(0)$ discrepancies are more than twice the estimated uncertainties. For the binding loop residues, the largest excesses occur for Thr44 and Asp46, in which the model-free values exceed the experimental $J(0)$ values by 0.14 and 0.10 ns/rad, respectively. For residues Glu2–Lys8, the model-free values exceed the experimental values by 0.09–0.14 ns/rad.

The types of discrepancies observed between the experimental and Lipari and Szabo spectral density values could be due in part to systematic errors in the relaxation rate measurements. For example, it has been shown that cross-relaxation pathways between one-spin and two-spin orders can occur due to the correlated motions of the NH bond vector and symmetry axis of $^{15}N$ chemical shift tensor (Boyd et al., 1990; Palmer et al., 1991a,b; Kay et al., 1991). The $R_N(N_z)$ and $R_N(N_{x,y})$ experiments are tailored to be free from the effects of these cross-correlations. However, the $R_{NH}$ $(2H_z^NN_{x,y})$ and $R_{NH}(2H_z^NN_z)$ experiments are not, and as a result, the recorded values may be too small. The two-spin terms are expected to be less affected by the cross-correlations than the analogous one-spin terms due to the effects of homonuclear amide proton relaxation. Equations 13–17 reveal that underestimations of $R_{NH}(2H_z^NN_{x,y})$ and $R_{NH}(2H_z^NN_z)$ will result in smaller $J(0)$ and $J(\omega_N)$ values and larger $J(\omega_{H^N}+\omega_N)$, $J(\omega_{H^N})$, and $J(\omega_{H^N}-\omega_N)$ values. Thus, the systematic discrepancies seen between the experimental and Lipari and Szabo spectral density values may be associated with residual cross-correlation effects.

The amide proton spin–lattice relaxation rate $[R_H(H_z^N)]$ measurements are another potential source of systematic error. Specifically, proton homonuclear cross-relaxation (Macura & Ernst, 1980) during the relaxation delay causes multiexponential relaxation of the amide proton magnetization. A single-exponential fit is only valid if the effects of proton–proton cross-relaxation are negligible compared to the direct relaxation rates. In the pulse sequence used to measure $R_H(H_z^N)$ two features help reduce the proton–proton cross-relaxation effects (Peng & Wagner, 1992). First, the pulse phases are cycled such that only amide protons experience inversion during the relaxation delay; all *non*-amide protons are flipped back to the $+z$ axis for all scans at the start of the relaxation delay. Second, the amide proton inversion is done only after the amide $^{15}N$ chemical shift labeling. This has the effect of inverting the different amide protons at different times according to the chemical shift of their bonded $^{15}N$ nucleus. As a result of these two features, the pulse sequence approximates a selective proton $T_1$ experiment for the individual amide protons. In such selective $T_1$ experiments, it becomes possible to estimate the individual direct relaxation rates $R_H(H_z^N)$ for sufficiently short relaxation delays. One gauge of the shortness of relaxation delays is given by the relative intensity of the NOE cross-peaks to the direct $^{15}N$–$^1H$ correlation peaks. At the longest relaxation delay of 125 ms, the amide–amide NOE cross-peaks were $\leq 5\%$ of the direct correlation peaks with the peak intensities still increasing. Thus, the effects of the proton–proton cross-relaxation do not appear to be serious in this time regime. Nonetheless, we have also fit the decay of the direct correlation peaks to a second-order polynomial adapted from the Taylor series expansion of the rigorous relaxation matrix solution given by Macura and Ernst (1980). The infinite Taylor series expansion has the advantage that relaxation and cross-relaxation can be rigorously separated. Here, the first three terms of the expansion are used, giving the three-parameter expression $I(T) = A(1 - R_H(H_z^N)T + {}^1/_2BT^2)$. $I(T)$ is the peak intensity as a function of relaxation delay $T$, $A$ represents the initial peak intensity value, $R_H(H_z^N)$ is the desired relaxation rate, and $B$ is a parameter designating the net spin–diffusion effects arising from proton–proton cross-relaxation. In most cases, the differences between the polynomial and exponential fits are on the same order as the estimated uncertainties ($\approx 7\%$) in the single-exponential fits. However, significant differences exist for some residues where the polynomial fit gives values that differ by 10–20%. Proton–proton cross-relaxation may be expected to introduce systematic underestimations of $R_H(H_z^N)$ values. In turn, eqs 13–17 show that smaller values of $R_H(H_z^N)$ will lead to overestimations of $J(0)$ and $J(\omega_N)$ and underestimations of $J(\omega_{H^N}+\omega_N)$, $J(\omega_{H^N})$, and $J(\omega_{H^N}-\omega_N)$. Furthermore, eqs 13–17 show that the $J(\omega)$ values most sensitive to variations in $R_H(H_z^N)$ are concentrated in the three higher frequency values. Clearly, more accurate measurements of $R_H(H_z^N)$ would be desirable to better gauge the effect of the homonuclear cross-relaxation on the extracted $J(\omega)$ values. It should be possible to obtain more accurate estimates using selective pulse techniques; these studies are in progress.

Thus, cross-relaxation effects due to either CSA–dipolar cross-correlations or proton–proton dipolar interactions may introduce systematic errors into the two-spin relaxation rates, $R_{NH}(2H_z^NN_{x,y})$, $R_{NH}(2H_z^NN_z)$, and the amide proton spin–lattice relaxation rate, $R_H(H_z^N)$. However, we note from eqs 13–17 that the expressions for the $J(\omega)$ values fortuitously involve differences of these rates. Therefore, systematic underestimations in these rates will tend to cancel to some extent. Nevertheless, the residual systematic errors may explain the discrepancies between the experimental values of $J(\omega)$ and those derived from the Lipari and Szabo approach. They may also explain the anomalous increase of the $J(\omega)$ values at high frequency.

Another possibility is that the model for the spectral density in the Lipari and Szabo approach, $J(\omega)_{ls}$, may be inadequate for certain types of NH vector motion. For example, the heteronuclear NOEs predicted by $J(\omega)_{ls}$ tend to be stronger than those observed in experiment. For 13 residues, the NOEs are overestimated by 20–75%; this greatly exceeds the typical experimental uncertainty of $\approx 7\%$. Generally, $J(\omega)_{ls}$ predicted stronger NOEs for residues that had smaller $R_N(N_{x,y})$/

$R_N(N_z)$ ratios and weaker NOEs for residues with larger $R_N(N_{x,y})/R_N(N_z)$ ratios. The predicted $R_N(N_{x,y})$ and $R_N(N_z)$ values matched the experimental data much better, although somewhat larger errors occurred for the $R_N(N_z)$ values. The overestimations of the NOEs may be due to an underestimation of $J(\omega_{H^N}-\omega_N)$ relative to $J(\omega_{H^N}+\omega_N)$ or an underestimation of $J(\omega_N)$ in eq 22. If so, the form of $J(\omega)_{ls}$ shown does not adequately describe the NH bond dynamics for these cases. We note that in cases where the effective internal correlation times $\tau_e$ were <25 ps, the predicted relaxation data were typically in much better agreement with the experimental data. Thus, the form of $J(\omega)$ in eq 22 may be less applicable when the internal motion time scale is no longer in the extreme-narrowing limit. Clearly, additional sampling points of $J(\omega)$ would be useful in addressing this problem. The potential inapplicability of $J(\omega)_{ls}$ for certain kinds of NH motion has already been discussed in a $^{15}N$ relaxation study of interleukin 1$\beta$ (Clore et al., 1990a,b). In those studies, an additional order parameter $S_f^2$ is introduced such that the original generalized order parameter is the product $S^2 = S_f^2 S_s^2$. The subscripts f and s refer to fast and slow internal motions, thus allowing for internal motions on two separate time scales. If the faster internal motion is characterized by a sufficiently small effective correlation time (e.g., <10 ps), then the only new fitting parameter introduced into $J(\omega)_{ls}$ is $S_f^2$. The inclusion of $S_f^2$ allows the interleukin 1$\beta$ relaxation data to be fit more adequately. While additional motional parameters may reduce the errors in the model-predicted relaxation parameters, the resulting model of $J(\omega)$ may or may not be more physically correct. Since our emphasis here has been to extract the $J(\omega)$ values from the relaxation parameters themselves, we have not included an $S_f^2$ analysis in the present study. Note that the distinct advantage of the spectral density mapping technique is that any errors in the motional interpretations stem only from the experimental data. In contrast, when using motional models, the errors stems not only from experimental error but also from potentially incorrect assumptions about the motion.

It is of interest to compare the behavior of the $J(\omega)$ values with the results of the solution structure determinations for eglin c (Hyberts & Wagner, 1990; Hyberts et al., 1992). There is a strong correlation between the backbone regions with low structural precision and those regions with low values of $J(0)$ and $J(\omega_N)$. In particular, significantly larger rmsds exist for the N-terminal residues and proteinase binding loop residues in the ensemble of calculated solution structures. This is evident in the bundle of structures shown in Figure 2. The higher frequency $J(\omega)$ values lack this correlation, since these values showed little variation with the protein sequence (see Figure 3). The correlation observed between $J(0)$, $J(\omega_N)$, and the backbone rmsds illustrates the complementary role the spectral density studies have to the structural studies of eglin c. Specifically, from the structural studies alone, one might conclude that the larger rmsds are a result of increased intramolecular motion. This conclusion would be premature, since the lack of structural definition more directly indicates a lack of structural constraints. While a lack of constraints may be due to internal mobility, other factors may contribute as well. Hence, the $J(\omega)$ data provide independent evidence that at least some of the structural ambiguity can be clearly associated with internal motion. It follows that no single structure can adequately define the protein backbone in these mobile regions. Thus, in general, caution is indicated in efforts to constrain poorly defined regions of solution structures, since the presence of internal mobility may limit the precision that should be aimed for.

The more rapid motions of the proteinase binding loop NH vectors are of significant interest when one considers the inhibitory function of eglin c. In the inhibitor–proteinase complex, the loop becomes enclosed in the proteinase–inhibitor interface (McPhalen et al., 1985; McPhalen & James, 1987). The structural studies suggest a segmental motion of the loop for free eglin c. Specifically, the backbone dihedral angles are poorly defined at residues 40 and 47 but well-defined for the intervening residues. The larger deviations of the binding loop suggest a hinge motion of the loop relative the more rigid protein core (Hyberts et al., 1992). The $J(\omega)$ data cannot directly probe for the existence of such correlated motions along the protein backbone. Nonetheless, the hypothesis of segmental motion is supported by the similar decreases in the $J(0)$ and $J(\omega_N)$ values for residues Val43–Leu47 and the quick return to the protein core values at Arg48. Segmental motion may enhance eglin c's proteinase binding capacity by allowing the loop to carry out a dynamic search for the proteinase binding pocket. Rigid body motion of the loop may allow the loop binding to be specific without sacrificing adaptability. Relaxation studies of an eglin c mutant, in which specific residues in the proteinase binding loop are substituted, appear to corroborate this hypothesis. This work will be presented elsewhere.

In summary, we have used the technique of mapping the spectral density functions directly from NMR relaxation parameters to analyze the backbone dynamics of eglin c. The technique differs from previous approaches in that no a priori model assumptions about the spectral density functions have been made. It has been shown that for residues involved in secondary structure the $J(\omega)$ values at high frequency (≥450 MHz) are much smaller than $J(0)$ and $J(\omega_N)$, confirming popular assumptions. For residues with significant internal motion, this is no longer true as $J(0)$ and the higher frequency values become more equal. In this study, the presence of internal motion is best probed by $J(0)$ and $J(\omega_N)$. It is conceivable that $J(\omega)$ in the wide range of frequencies between 50 and 450 MHz may prove interesting for probing internal dynamics. $J(\omega)$ can be mapped in this domain by applying these methods using either different field strengths or different nuclei. Comparison of the spectral density values with those predicted by the popular Lipari and Szabo formalism shows similar results for residues with high order parameters ($S^2$ close to 1.0) and larger discrepancies for residues with lower order parameters. Some of these discrepancies are due to the aforementioned irregular behavior of the higher frequency spectral densities; work is in progress at different field strengths to clarify the origin of these irregularities. Significantly larger mobility has been demonstrated for the N terminus and proteinase binding loop of eglin c. These regions are characterized by broader spectral density functions of smaller amplitude, indicating a greater contribution of higher frequency motions compared to the protein core. These regions also correspond to the low-precision regions in the NMR structure determinations of eglin c and therefore give independent evidence that the low precision of these regions can be associated with the existence of significant internal motion. This demonstrates the complementary nature of the dynamics and structural studies.

## ACKNOWLEDGMENT

We are indebted to Drs. Dirk Heinz and Markus Grütter, Ciba-Geigy, Basel, Switzerland, for the gift of [$^{15}N$]eglin c. We express our appreciation to Mr. S. G. Hyberts for fruitful discussions and preparation of Figure 2. We thank Drs. V. Thanabal and C. J. Kördel and Mr. R. T. Clubb for useful

discussions. We also thank Drs. Mark Rance and L. E. Kay for sending preprints of their work prior to publication. We are grateful to Dr. Dennis Hare for providing the data processing software package FELIX.

## SUPPLEMENTARY MATERIAL AVAILABLE

Two tables listing all six relaxation rates [$R_N(N_z)$, $R_N(N_{x,y})$, $R_{NH}(2H_z^N N_{x,y})$, $R_{NH}(2H_z^N N_z)$, $R_H(H_z^N)$, $R_N(H_z^N \rightarrow N_z)$] and NOEs along with the estimated errors for each analyzed residue and the five spectral density values [$J(0), J(\omega_N), J(\omega_{H^N}-\omega_N), J(\omega_{H^N}), J(\omega_{H^N}+\omega_N)$] extracted from the relaxation data and the associated errors for each analyzed residue (5 pages). Ordering information is given on any current masthead page.

## REFERENCES


Abragam, A. (1961) *The Principles of Nuclear Magnetism*, Clarendon Press, Oxford, England.

Allerhand, A., Doddrell, D., Glushko, V., Cochran, D. W., Wenkert, E., Lawson, P. J., & Gurd, F. R. N. (1971) *J. Am. Chem. Soc. 93*, 544–546.

Bax, A., Ikura, M., Kay, L. E., Torchia, D. A., & Tschudin, R. (1990) *J. Magn. Reson. 86*, 304–318.

Bode, W., Papamokos, D., Musil, D., Seemüller, U., & Fritz, H. (1986) *EMBO J. 5*, 813–818.

Bode, W., Papamokos, E., & Musil, D. (1987) *Eur. J. Biochem. 166*, 673–692.

Boyd, J., Hommel, U., & Campbell, I. D. (1990) *Chem. Phys. Lett. 175*, 477–482.

Brooks, C. L., Karplus, M., & Pettitt, B. M. (1988) *Adv. Chem. Phys. 71*, 1–259.

Brünger, A. T., Clore, G. M., Gronenborn, A. M. & Karplus, M. (1986) *Proc. Natl. Acad. Sci. U.S.A. 83*, 3801–3805.

Chandler, D. (1987) *Introduction to Modern Statistical Mechanics*, Oxford University Press, New York.

Clore, G. M., & Gronenborn, A. M. (1989) *CRC Crit. Rev. Biochem. 24*, 479–564.

Clore, G. M., Szabo, A., Bax, A., Kay, L. E., Driscoll, P. C., & Gronenborn, A. M. (1990a) *J. Am. Chem. Soc. 112*, 4989–4991.

Clore, G. M., Driscoll, P. C., Wingfield, P. T., & Gronenborn, A. M. (1990b) *Biochemistry 29*, 7387–7401.

Dellwo, M. J., & Wand, A. J. (1989) *J. Am. Chem. Soc. 111*, 4571–4578.

Ernst, R. R., Bodenhausen, G., & Wokaun, A. (1987) *Principles of Nuclear Magnetic Resonance in One and Two Dimensions*, Oxford University Press, Oxford, England.

Friedman, H. L. (1985) *A Course In Statistical Mechanics*, Prentice-Hall, Englewood Cliffs, NJ.

Goldman, M. (1988) *Quantum Description of High-Resolution NMR in Liquids*, Clarendon Press, Oxford, England.

Heinz, D. W., Hyberts, S. G., Peng, J. W., Priestle, J. P., Wagner, G., & Grütter, M. G. (1992) *Biochemistry* (submitted for publication).

Hiyama, Y., Niu, C., Silverton, J. V., Bavaso, A., & Torchia, D. A. (1988) *J. Am. Chem. Soc. 110*, 2378–2383.

Hyberts, S. G., & Wagner, G. (1990) *Biochemistry 29*, 1465–1474.

Hyberts, S. G., Goldberg, M. S., Havel, T. F., & Wagner, G. (1992) *Protein Science 1*, 736–751.

Jardetzky, O., & Roberts, G. C. K. (1981) *NMR in Molecular Biology*, Academic Press, New York.

Johnson, M. (1985) *Anal. Biochem. 148*, 471–478.

Kamath, U., & Shriver, J. W. (1989) *J. Biol. Chem. 264*, 5586–5592.

Karplus, M., & McCammon, J. A. (1981) *CRC Crit. Rev. Biochem.*, 293–349.

Kay, L. E., Torchia, D. A., & Bax, A. (1989) *Biochemistry 28*, 8972–8979.

Kay, L. E., Nicholson, L. K., Delaglio, F., Bax, A., & Torchia, D. A. (1991) *J. Magn. Reson.* (in press).

Keiter, E. A. (1986) Ph.D. Thesis, University of Illinois.

King, R., & Jardetzky, O. (1978) *J. Chem. Phys. Lett. 55*, 15–18.

King, R., Maas, R., Gassner, M., Nanda, R. K., Conover, W. W., & Jardetzky, O. (1978) *Biophys. J. 6*, 103–117.

Kinoshita, K., Kawato, W., Jr., & Ikegami, A. (1977) *Biophys. J. 20*, 289.

Lipari, G., & Szabo, A. (1982a) *J. Am. Chem. Soc. 104*, 4546–4559.

Lipari, G., & Szabo, A. (1982b) *J. Am. Chem. Soc. 104*, 4559–4570.

Macura, S., & Ernst, R. R. (1980) *Mol. Phys. 41*, 95–117.

Marion, D., & Wüthrich, K. (1983) *Biochem. Biophys. Res. Commun. 113*, 967–974.

Märki, W., Rink, H., Schnebli, H. P., Liersch, M., Raschdorf, F., & Richter, W. (1985) in *Peptides: Structure and Function, Proceedings of the 9th American Peptide Symposium* (Deber, C. M., Hruby, V. J., & Kopple, K. D., Eds.) pp 385–388, Pierce Chemical Co., Rockford, IL.

Marquardt, D. W. (1963) *J. Soc. Ind. Appl. Math. 11*, 431–441.

McCammon, J. A., & Harvey, S. C. (1987) *Dynamics of Proteins and Nucleic Acids*, Cambridge University Press, New York.

McPhalen, C. A., & James, M. N. G. (1987) *Biochemistry 26*, 261–269.

McPhalen, C. A., & James, M. N. G. (1988) *Biochemistry 27*, 6582–6598.

McPhalen, C. A., Schnebli, H. P., & James, M. N. G. (1985) *FEBS Lett. 188*, 55–58.

Nilges, M., Clore, G. M., & Gronenborn, A. M. (1988a) *FEBS Lett. 239*, 129–136.

Nilges, M., Clore, G. M., & Gronenborn, A. M. (1988b) *FEBS Lett. 239*, 317–324.

Nirmala, N. R., & Wagner, G. (1988) *J. Am. Chem. Soc. 110*, 7557–7558.

Nirmala, N. R., & Wagner, G. (1989) *J. Magn. Reson. 82*, 659–661.

Noggle, J. H., & Schirmer, R. E. (1971) *The Nuclear Overhauser Effect*, Academic Press, New York.

Palmer, A. G., III, Rance, M., & Wright, P. E. (1991a) *J. Am. Chem. Soc. 113*, 4371–4380.

Palmer, A. G., III, Skelton, N. J., Chazin, W. J., Wright, P. E., & Rance, M. (1991b) *Mol. Phys. 75*, 699–711.

Peng, J. W., & Wagner, G. (1992) *J. Magn. Reson. 98*, 308–332.

Peng, J. W., Thanabal, V., & Wagner, G. (1991a) *J. Magn. Reson. 94*, 82–100.

Peng, J. W., Thanabal, V., & Wagner, G. (1991b) *J. Magn. Reson. 95*, 421–427.

Press, W. H., Flannery, B. P., Teukolsky, S. A., & Vetterling, W. T. (1988) *Numerical Recipes in C—The Art of Scientific Computing*, Cambridge University Press, New York.

Ribeiro, A. A., King, R., Restivo, C., & Jardetzky, O. (1980) *J. Am. Chem. Soc. 102*, 4040–4051.

Richarz, R., Nagayama, K., & Wüthrich, K. (1980) *Biochemistry 19*, 5189–5196.

Shaka, A. J., Barker, P. B., & Freeman, R. (1985) *J. Magn. Reson. 64*, 547–552.

Slichter, C. P. (1978) *Principles of Magnetic Resonance*, Springer Verlag, New York.

Sørensen, O. W., Eich, M. H., Levitt, M. H., Bodenhausen, G., & Ernst, R. R. (1983) *Prog. NMR Spectrosc. 16*, 163–192.

Wagner, G., & Nirmala, N. R. (1989) *Chem. Scr. 29A*, 27–30.

Wagner, G., Bodenhausen, G., Müller, N., Rance, M., Sørensen, O. W., Ernst, R. R., & Wüthrich, K. (1985) *J. Am. Chem. Soc. 107*, 6440–6446.

Wittebort, R. J., & Szabo, A. (1978) *J. Chem. Phys. 69*, 1723–1736.

Woessner, D. E. (1962) *J. Chem. Phys. 36*, 647–654.

Zare, R. N. (1988) *Angular Momentum*, Wiley, New York.


**Registry No.** Eglin c, 96380-69-7; nitrogen, 7727-37-9.